CHALMERS
UNIVERSITY OF TECHNOLOGY

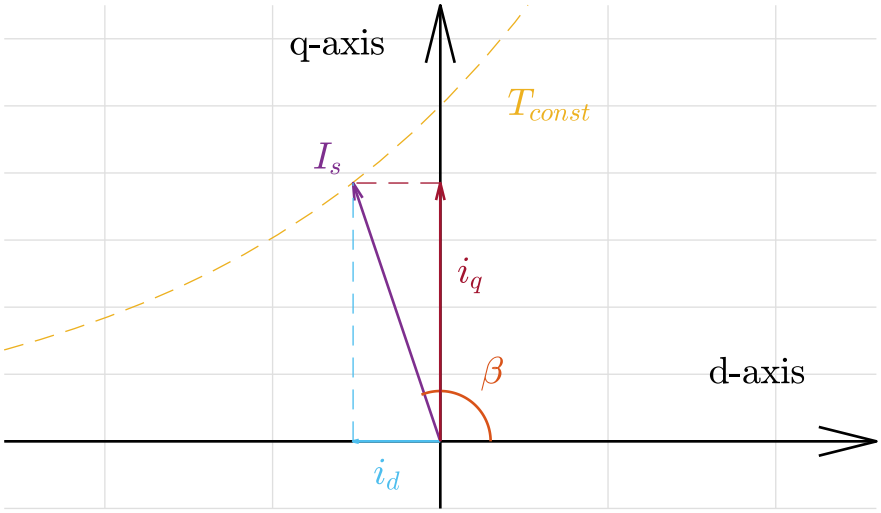

Adaptive Maximum Torque Per Ampere Control of IPMSM

Using Current Ripple measurement and Virtual Signal Injection combined with Model Reference Adaptive Control

Master's thesis in Systems, Control and Mechatronics

RICHARD BURGI
JAKOB LAURELL

Department of Electrical Engineering
CHALMERS UNIVERSITY OF TECHNOLOGY
Gothenburg, Sweden 2019

Master's thesis 2019

Adaptive Maximum Torque Per Ampere Control of IPMSM

Using Current Ripple measurement and Virtual Signal Injection combined with Model Reference Adaptive Control

RICHARD BURGI
JAKOB LAURELL

CHALMERS
UNIVERSITY OF TECHNOLOGY

Department of Electrical Engineering
Chalmers University of Technology
Gothenburg, Sweden 2019

Adaptive Maximum Torque Per Ampere Control of IPMSM
Using Current Ripple measurement and Virtual Signal Injection combined with Model Reference Adaptive Control
RICHARD BURGI
JAKOB LAURELL

Supervisor: Jonas Sjöberg, Chalmers University of Technology
Supervisor: Freddy Trinh, China Euro Vehicle Technology, CEVT
Examiner: Jonas Sjöberg, Chalmers University of Technology

Master's Thesis 2019
Department of Electrical Engineering
Chalmers University of Technology
SE-412 96 Gothenburg
Telephone +46 31 772 1000

Cover: Illustration of the Maximum Torque Per Ampere (MTPA) concept in the dq-reference frame. A number of different current vectors, with components i_d and i_q, can produce the same amount of torque illustrated by the dashed yellow line, T_{const}. The target for a MTPA control strategy can be formulated as minimizing the current amplitude I_s by choosing a proper current angle β.

Typeset in LaTeX
Gothenburg, Sweden 2019

Adaptive Maximum Torque Per Ampere Control of IPMSM
Using Current Ripple measurement and Virtual Signal Injection combined with Model Reference Adaptive Control
RICHARD BURGI
JAKOB LAURELL
Department of Electrical Engineering
Chalmers University of Technology

Abstract

With the electrification in the automotive industry, the popularity of Interior Permanent Magnet Synchronous Machines (IPMSMs) is increasing. Optimizing the efficiency in the low speed region is commonly known as tracking the MTPA operations. However, as the motor parameters changes with inductance saturation, stator temperature variations and aging of the machine, the problem of tracking MTPA becomes a challenging task. This thesis aims to solve the problem with a fully adaptive algorithm that does not require prior knowledge of the machine and provides both accurate speed- and MTPA- tracking.

The proposed algorithm combines three state of the art methods, Adaptive Control, Parameter Identification using current ripple measurements, and Virtual Signal Injection, to enable adaptive MTPA tracking in real time. Full motor parameters' estimation without any prior knowledge of the machine are performed using a Model Reference Adaptive Controller MRAC in combination with current ripple measurements. Additional MTPA accuracy is achieved through Look-up-Table (LuT) data which is used in combination with a VSI scheme in order to estimate the derivatives of the parameters with respect to the current angle, adding factors which are often neglected.

The final algorithm is tested in a simulation environment using Simulink and shows superior MTPA tracking in comparison with a default algorithm currently evaluated at China Euro Vehicle Technology AB (CEVT). The proposed control scheme tracks the parameter variations in real time and the MTPA tracking is showing high performance even at varying motor temperature conditions.

Keywords: Maximum Torque Per Ampere (MTPA), Current Ripple, Virtual Signal Injection (VSI), Model Reference Adaptive Control (MRAC), Real Time Parameter Estimations, Interior Permanent Magnet Synchronous Machine (IPMSM)

Contents

List of Figures

Acronyms

CEVT China Euro Vehicle Technology AB.

DC Direct Current.

emf Electromotive force.

FEA Finite Element Analysis.
FW Flux-weakening.

IM Induction Machine.
IMC Internal Model Control.
IPMSM Interior Permanent Magnet Synchronous Machine.

LuT Look-up-Table.

MRAC Model Reference Adaptive Control.
MTPA Maximum Torque Per Ampere.
MTPV Maximum Torque Per Voltage.

PE Power Electronics.
PI Proportional Integral.

RLS Recursive Least Squares.

VSI Virtual Signal Injection.

WLTP Worldwide harmonized Light vehicles Test Procedure.

Nomenclature

α	IMC current controller time constant
β	Stator current angle to d-axis
β^h	Current angle with injected high frequency component
β_{MTPA}	MTPA current angle
$\dot{\boldsymbol{e}}$	Current error derivative vector
$\hat{\boldsymbol{\theta}}$	Estimated parameter deviation vector
$\hat{\boldsymbol{d}}$	Estimated model error vector
$\hat{\boldsymbol{e}}$	Current error vector between reference current and reference model current
$\hat{\boldsymbol{G}}$	Reference model plant transfer function
$\hat{\boldsymbol{i}}$	Reference model current vector
$\boldsymbol{\Lambda}$	Adaption law matrix gain
$\boldsymbol{\theta}$	Parameter vector for RLS algorithm
$\boldsymbol{\theta}$	RLS algorithm parameter vector
$\tilde{\boldsymbol{d}}$	Difference between real and estimated model error
$\tilde{\boldsymbol{u}}$	Adaption law input vector
$\boldsymbol{\varphi}$	RLS algorithm system matrix
$\boldsymbol{A_0}$	Reference model system matrix
$\boldsymbol{A}$	Plant model system matrix
$\boldsymbol{B_0}$	Reference model input matrix
$\boldsymbol{B}$	Plant model input matrix
$\boldsymbol{C}$	Generic controller transfer function
$\boldsymbol{d}$	Model error vector
$\boldsymbol{i}^*$	Current reference vector
$\boldsymbol{I}$	Identity matrix
$\boldsymbol{K}$	RLS algorithm matrix gain
$\boldsymbol{k}$	Adaption law matrix gain
$\boldsymbol{P}$	RLS algorithm matrix gain
$\boldsymbol{T_\sigma}$	Time constant matrix
$\boldsymbol{T_i}, \boldsymbol{T_n}$	General PI controller time constants
$\boldsymbol{T_m}$	Time constant matrix
$\boldsymbol{T}$	Symmetrical Optimum transfer function
$\boldsymbol{u}_e^e$	Back-emf error vector
$\boldsymbol{u_e}$	Input consisting of decoupled terms for the plant model
$\boldsymbol{u_s}$	Voltage input vector
$\boldsymbol{y}$	RLS algorithm input vector
$\Delta\psi_m$	Permanent magnet flux deviation from nominal value

$\Delta I_{d,i}, \Delta I_{q,i}$	dq-axis current variation within switching section i
$\Delta L_d, \Delta L_q$	dq-axis inductance deviation from nominal value
ΔR_s	Stator resistance deviation from nominal value
$\Delta u_d, \Delta u_q$	Resulting dq-axis voltage component variation from parameter variations and current ripple
$\dot{i}_d, \dot{i}_q$	dq-axis current derivative
$\dot{V}$	Lyapunov function derivative
$\dot{\hat{i}}_d, \dot{\hat{i}}_q$	dq-axis reference model current derivative
ϵ_d, ϵ_q	dq-axis model uncertainties
$\hat{\cdot}$	Estimated quantity
$\hat{\Psi}_d, \hat{\Psi}_q$	dq-axis flux linkage estimation
$\hat{d}_d, \hat{d}_q$	Estimated dq-axis model error
$\hat{i}_d, \hat{i}_q$	dq-axis reference model current
$\boldsymbol{\hat{u}_e}$	Input consisting of decoupled terms for the reference model
$\boldsymbol{\hat{u}}$	Reference model voltage input
λ	RLS algorithm forgetting factor
λ_d, λ_q	Adaption law matrix diagonal components
ω	Electrical motor speed
ω_c	Current ripple speed filter time constant
ω_h	Frequency of injected sinusoidal
ω_s	General second order system time constant
Ψ_d, Ψ_q	dq-axis flux linkage
ψ_m	Permanent magnet flux
ψ_m^h	Resulting permanent magnet flux from injected high frequency component
ψ_{m0}	Nominal permanent magnet flux
θ	Rotor angle
θ_v	Voltage vector angle
φ_d, φ_q	dq-axis phase delays
ζ	General second order system damping coefficient
A_d, A_q	dq-axis current ripple amplitude
A_h	Magnitude of injected sinusoidal
D	Symmetrical optimum transfer function denominator
e_ω	Speed error signal
e_d, e_q	dq-axis current error
$i^m_{d(q),ripple}$	Measured dq-axis current ripple components
i_d, i_q	dq-axis stator current
i^*_d, i^*_q	dq-axis current reference
i^h_d, i^h_q	Filtered dq-current ripple components
i^h_d, i^h_q	dq-axis stator currents with injected high frequency component
I_s	Stator current magnitude
$i_{d,ripple}$	d-axis current ripple component
$i_{d,f}, i_{q,f}$	dq-axis current fundamental components
$i_{q,ripple}$	q-axis current ripple components
J	Rotor inertia
j	Imaginary unit

k_d, k_q	Adaption law matrix diagonal components
$K_{q,i}, K_{q,i}$	dq-axis reference current controller integral gain
$K_{q,p}, K_{q,p}$	dq-axis reference current controller proportional gain
L_d, L_q	dq-axis stator inductance
L_{d0}, L_{q0}	dq-axis nominal stator inductance
n	Discrete time step
p	Number of pole-pairs in the rotor
R_s	Stator winding resistance
R_{s0}	Nominal stator resistance
s	Laplace variable
T	Temperature
t	Time
T_c	Torque derivative constant parameter component
T_d	Torque derivative parameter derivative component
T_e	Electric torque produced by IPMSM
T_e^h	Resulting electrical torque with high frequency injected signal
T_e^{ref}	Electric torque reference
t_i	Switching time for switching section i
T_L	Load torque
T_m, T_σ	d-axis components of time constant matrices
t_r	System rise time
T_s	Sample time
$T_{d,s}, T_{q,s}$	dq-axis reference current controller time constant
t_{est}	RLS algorithm sample time
u_d, u_q	dq-axis voltage
$u_{d,i}, u_{q,i}$	dq-axis voltage components during switching section i
V	Lyapunov function
z	z-transform variable

1

Introduction

The electrification of the automotive industry puts the engineers up for new challenges. The traditional combustion powertrains are being replaced by hybrid solutions and fully electrical powertrains. Within the industry, IPMSMs are widely adopted because of their high efficiency, high power density and high reliability compared to DC- and Induction Machines (IMs) [1].

IPMSMs belong to the family of synchronous motors and are characterized by having permanent magnets buried inside the rotor. By applying a alternating voltage to the stator windings, a rotating magnetic field is generated. The interaction between the magnetic properties of the rotor and the applied magnetic field causes the motion of the rotor. The frequency at which the rotor rotates is proportional to the supplied voltage's frequency and the number of pole pairs in the rotor [2].

IPMSMs are often described in the abc-frame or in the synchronous dq-frame, see Figure 1.1. While the abc-frame is fixed to the stator, the dq-frame is fixed to the rotor. The d-axis of the dq-frame is aligned with the magnetic field of the permanent magnet and the q-axis is separated from the d-axis with 90 electrical degrees. The electrical angle is related to the mechanical angle based on the number of pole pairs [1]. The mechanical angle of the rotor, θ, is defined as the angle between the phase a axis and the d-axis as seen in Figure 1.1.

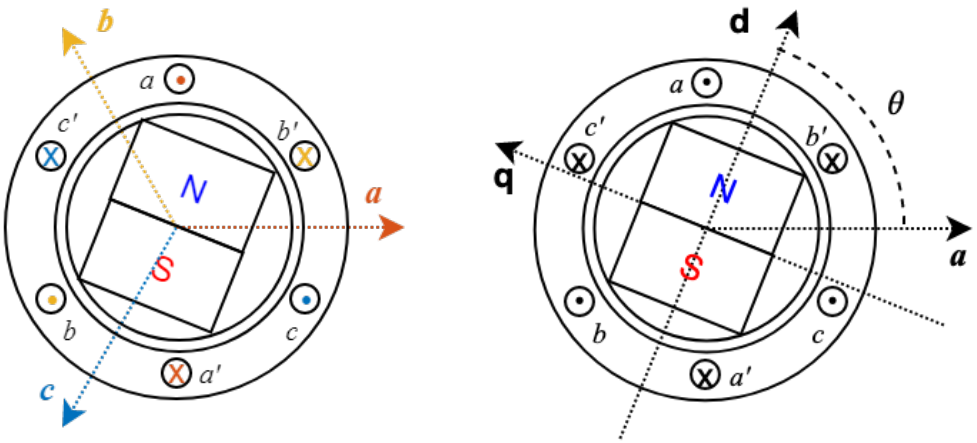

(a) abc-frame **(b)** Synchronous dq-frame

Figure 1.1: Schematic representation of an IPMSM, here with only one permanent magnet.

The three-phase supply current can thus be described in the dq-frame using the Park transformation, the details of which are given in Appendix A. In the dq-frame the three-phase supply current is represented as a current vector of magnitude I_s and angle β with respect to the d-axis. The current can thus be split into one component in each axis direction i_d, i_q as seen in Figure 1.2.

An important property of the IPMSM is that the rotor is asymmetrical and therefore has different magnetic properties along the d- and q-axis directions. Since the permanent magnet permeability is close to the permeability of air, the d-axis magnetic permeance is much lower than the q-axis permeance [3]. This enables the production of a reluctance torque in addition to the magnetic torque, which is generated as a result of the permanent magnet flux ψ_m. In the rotating reference frame, the anisotropy is characterized by the d- and q-axis inductances L_d and L_q.

The magnetic torque depends on the i_q current while the reluctance torque is proportional to the product of the i_d and i_q currents. Hence, there are an infinite number of current vectors that can produce the same amount of torque. This is illustrated with the dashed yellow line that represent a constant torque level in Figure 1.2.

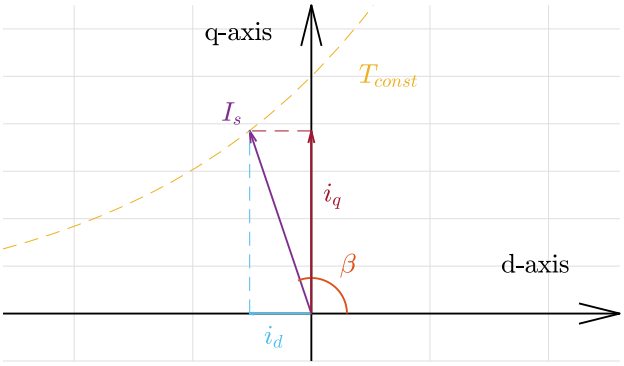

Figure 1.2: Illustration of stator currents in the dq-reference frame. T_{const} shows typical characteristics of a constant torque curve.

Within powertrain applications, the IPMSMs are generally controlled based on their rotational speed ω. The reference speed input is typically generated from other control systems within the vehicle [4]. The task of the motor controller is to generate the i_d and i_q currents to produce the torque required to reach the reference speed.

When an electric motor is operating below its rated speed, the problem of optimizing the efficiency can therefore be formulated as finding the dq-current combination that generates the requested torque with minimum current amplitude I_s. Which can be done by selecting the proper current angle β. This problem is commonly known as finding the MTPA and was introduced in [5].

Above the rated rotational speed, MTPA can not be used as a control strategy as the maximum power of the motor limits the torque production at high speeds. Instead, other techniques, such as Maximum Torque Per Voltage (MTPV) and Flux-weakening (FW), are used to control the motor in this region.

In order to find the MTPA at a given torque, accurate knowledge of the motor parameters L_d, L_q and ψ_m are needed. However, the motor parameters are sensitive to the operating conditions and varies due to inductance saturation, temperature changes and aging of the machine [6]. Although measurements of these parameters are often provided by the supplier, these measurements cannot handle the long term variation.

In the literature, a number of different methods are used to control IPMSM efficiently with MTPA operations [7, 8, 9]. A common approach is using Adaptive Control to handle the parameter variations and maintain good control performance in the entire operation range. In [7], a Model Reference Adaptive Control (MRAC) scheme is combined with a parameters identification technique in order to control the motor with MTPA operations. However, only two equations are obtained for the parameter identification scheme and hence the algorithm is only able to estimate two of the motor parameters. In [8], current ripple measurement is used to expand the parameter identification scheme with two additional equations and thereof solving the rank-deficiency problem. The paper shows accurate parameter estimation results but the MTPA tracking is still insufficient due to the neglection of the variation of the motor parameters with respect to the current angle β. Another type of methods is extremum seeking control in the form of Virtual Signal Injection [9]. These method can track MTPA accurately but suffers from slow response and are therefore problematic as stand alone solutions for real time applications. These and other state of the art methods are described in detail in Section 2.4.

1.1 Motivation

This Master's Thesis has been performed at the Powertrain Engineering team at CEVT, which is responsible for the development of the propulsion systems and the controls associated with these systems. The Propulsion Control Team is currently working on the development of control systems for a new global hybrid transmission system, from the early concept phase to industrialization. The aim is that this transmission system should be used as one of the main technologies within the Geely group. A substantial task within the hybrid transmission system development is optimizing the efficiency of the electric machines.

For the time being, CEVT is evaluating a default algorithm, provided with the Hybrid Kit drive[1], to achieve MTPA operations. For the rest of the thesis, this algorithm will be referred to as the *Hybrid Kit algorithm*. Since this algorithm uses LuT for the motor parameters, it is not able to adapt to parameters' changes due to aging of the machine. The details of the algorithm is presented in Section 4.3. In this thesis, the performance of it will be used as a baseline for comparison.

1.2 Contributions

The main contribution of the thesis is the implementation of a controller that combines three state of the art methods, Adaptive Control, parameter identification us-

[1] https://www.infineon.com/cms/en/product/evaluation-boards/hybrid-kit-drive/

ing current ripple measurements and Virtual Signal Injection, in order to efficiently track MTPA operations in real time. The work has been limited to optimizing the efficiency in the low speed operating region of the IPMSM, where the MTPA operation is valid. Therefore, the thesis has not included FW nor high speed MTPV operation optimization. The transition from MTPA to FW control has also been ignored. An overview of the proposed control system can be seen in Figure 1.3

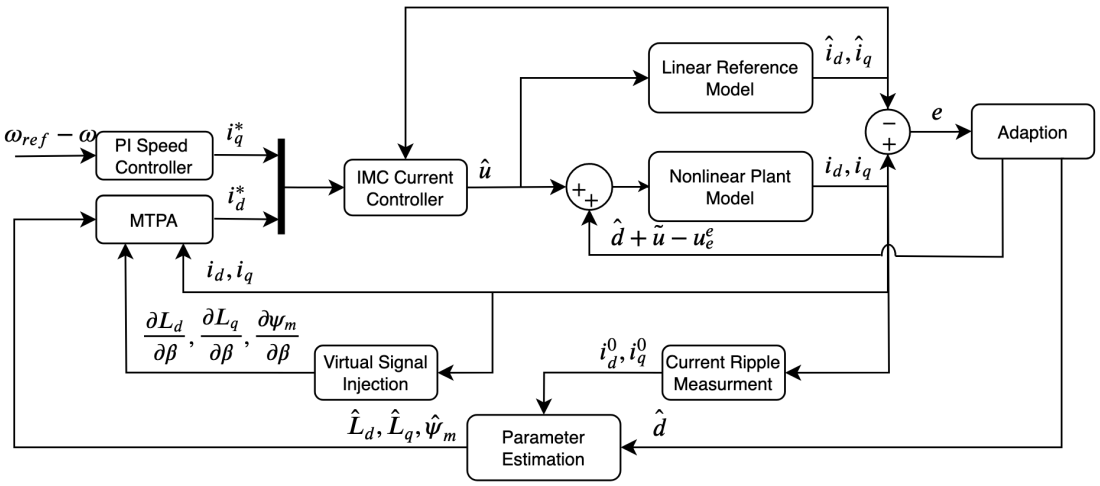

Figure 1.3: Overview of the proposed control system.

The proposed algorithm only rely on measurements which are available when the IPMSM is operating in a vehicle. That is the motor rotational speed, ω, currents and voltages measurements, i_d, i_q, u_d, u_q, which are further described in Section 2.1. The algorithm is tested in a simulation environment with a nonlinear plant model and additional sensor noise. The simulation results show that the proposed algorithm manages to estimate all motor parameters L_d,L_q and ψ_m without prior knowledge of their value. Moreover, using the VSI and parameters' LuT data, high MTPA tracking accuracy is achieved through parameter derivative estimations.

The purpose of the thesis can be summarized in the following questions which are answered throughout the report:

What current methods are used to track MTPA and which assumptions are they based on? Is it possible to combine the methods to improve performance while maintaining stability?

How well does the proposed algorithm perform compared with the true MTPA curve of the motor model and the default Hybrid Kit algorithm?

1.3 Sustainability aspects

As the main focus of the thesis is to investigate and develop an algorithm to maximize the efficiency of IPMSMs, the outcome may be applied in fields outside of the hybrid powertrain applications hence contributing to a more sustainable society.

With the increase popularity electric vehicles, it follows an increase in the demand of batteries. Although electric vehicles promise to reduce CO2 emission, the sustainable aspect of battery's production is still a subject of debate. In 2016, a research

from the Centre for Research on Multinational Corporations (SOMO), reported environmental pollution as a consequence of cobalt mining [10], one of the components of Lithium-ion batteries which are very common in the automotive industry.

1.4 Thesis outline

Chapter 2 presents the theoretical description of the IPMSM along with details of the parameter variations and challenges of the MTPA problem. The end of the chapter is focused around related work and explaining the details of the state of the art methods that this thesis is based on.

The details of the proposed control system is given in Chapter 3 where the development process of the complete system is explained step by step.

In Chapter 4 the evaluation process is described along with the details of the Hybrid Kit algorithm which will be used as a reference for comparison.

The results of the thesis is presented in Chapter 5 and a following discussion is given in Chapter 6.

Finally the outcome of the thesis is summarized in Chapter 7 along with some suggestions of future work.

2

Theoretical Background

In this chapter the mathematical model describing an IPMSM is presented. Based on the motor model, the MTPA relation is derived, followed by an analysis of the parameters' variations. Lastly, the state of the art methods, on which the proposed algorithm is based, are presented.

2.1 IPMSM model

The details of operation of an IPMSM was introduced in Chapter 1. Using the dq-frame the motor can be modeled with the equivalent circuits shown in Figure 2.1 [1]. The voltage equilibrium for each axis can thus be obtained as

$$\begin{aligned} u_d =& R_s i_d + L_d \frac{di_d}{dt} - \omega L_q i_q \,, \\ u_q =& R_s i_q + L_q \frac{di_q}{dt} + \omega (L_d i_d + \psi_m) \,, \end{aligned} \tag{2.1}$$

where $u_d, u_q, i_d, i_q, L_d, L_q$ are the voltages, currents and inductances in the d- and q-axis direction respectively, R_s is the stator winding resistance, ψ_m is the permanent magnet flux and ω is the electrical rotational speed.

The torque generated by an IPMSM can also be described as a function of the motor parameters as

$$T_e = \frac{3p}{2} \left[\psi_m + (L_d - L_q) i_d \right] i_q \,, \tag{2.2}$$

where p is the number of pole pairs.

In the following section, the obtained torque equation (2.2) will be used to derive the MTPA relation. The motor model (2.1) will further be used for the controller development in Chapter 3.

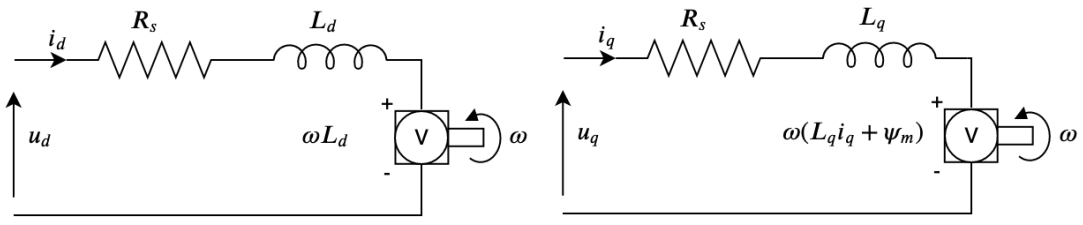

Figure 2.1: Equivalent circuit used for modelling the IPMSM.

2.2 Maximum Torque Per Ampere

From the torque relation in (2.2), a natural question to ask is how do we optimize the efficiency of the electric motor. A common optimization criteria is to minimize the current amplitude required to produce a given torque. This control strategy is commonly known as MTPA [5].

A natural approach to solving the MTPA problem is to take the derivative of (2.2) with respect to the current angle β and set it equal to zero as

$$\frac{\partial T_e(\beta)}{\partial \beta} = 0\,. \tag{2.3}$$

As seen in Figure 1.2, the stator current in the synchronous dq-frame can be expressed as

$$\begin{aligned} i_d =& I_s \cos(\beta)\,, \\ i_q =& I_s \sin(\beta)\,, \end{aligned} \tag{2.4}$$

where I_s is the current vector magnitude and β is the current angle. The left side of (2.3) can thus be expressed as

$$\frac{\partial T_e(\beta)}{\partial \beta} = T_c + T_d\,, \tag{2.5}$$

where

$$T_c = \frac{3}{2} p \left[\psi_m i_d + (L_d - L_q) i_d^2 - (L_d - L_q) i_q^2\right]\,, \tag{2.6}$$

and

$$T_d = \frac{3}{2} p \left[\frac{\partial \psi_m}{\partial \beta} i_q + \frac{\partial L_d}{\partial \beta} i_d i_q - \frac{\partial L_q}{\partial \beta} i_d i_q\right]\,. \tag{2.7}$$

Hence the MTPA relation (2.5) is split into two main parts. One which depends directly on the values of the parameters' and another part which depends on the parameters' derivative with respect to the current angle β.

It should be noted that MTPA only implies maximum efficiency in the case when the stator iron losses of the IPMSM are negligible in comparison to the copper losses of the windings [11]. Detailed mathematical expressions of these losses are given in [12]. From the equations in the paper, it can been seen that this assumption holds in the low speed region where MTPA is applicable. This statement is also verified in a simulation environment in [13] and is therefore not discussed further in this thesis.

2.3 Motor Parameter Variations

The motor parameters used to describe the motor characteristics in (2.1)-(2.2) are subject to change due to cross coupling effects, magnetic saturation, temperature dependency and aging of the machine [6].

The general motor parameters are hence given as

$$\begin{aligned} L_d &= L_d(i_d, i_q, T, t)\,, \\ L_q &= L_q(i_d, i_q, T, t)\,, \\ \psi_m &= \psi_m(i_d, i_q, T, t)\,, \\ R_s &= R_s(i_d, i_q, T, t)\,, \end{aligned} \tag{2.8}$$

or equivalently, using the current relations in (2.4), as

$$\begin{aligned} L_d &= L_d(I_s, \beta, T, t)\,, \\ L_q &= L_q(I_s, \beta, T, t)\,, \\ \psi_m &= \psi_m(I_s, \beta, T, t)\,, \\ R_s &= R_s(i_d, i_q, T, t)\,, \end{aligned} \tag{2.9}$$

where T is the temperature and t denotes time.

The cross coupling effect caused by the i_d and i_q currents is a rather quick phenomena as the current levels typically change within the order of 0.1-1 milliseconds. Temperature changes are typically slower, in the range of seconds, as the motor needs to operate at a high load for a short period of time to build up the internal temperature. Aging of the machine is the slowest process and significant parameter variations happens within months or even years. As the proposed control system, see Chapter 3, is based on the idea of estimating all parameters without prior knowledge of their variations, these time-frames sets the target of how fast the estimation must be.

In Figure 2.2 it is possible to see the variation of the motor parameters due to cross-coupling saturation used in the simulation motor model introduced in Section 4.1. The stator resistance R_s is assumed to be constant in the simulation motor model and hence only the other parameters are shown. The figure shows large variations for all three parameters of up to 45-75% compared to their value at $i_{d,q} = 0$. These variations are important to take into consideration when solving the MTPA equation as the large variations will have a significant effect on the optimal current angle.

2.4 State of the art methods

Commonly used methods for finding the optimal current angle β, i.e. solving the MTPA equation (2.3), can be divided into the following categories: numerical methods combined with LuTs, signal injection based methods and adaptive algorithms.

A common assumption for finding an analytical solution is to neglect the term T_d in (2.5) which yields the expression

$$\frac{\partial T_e(\beta)}{\partial \beta} \approx \frac{3}{2} p \left[\psi_m i_d + (L_d - L_q) i_d^2 - (L_d - L_q) i_q^2 \right] \tag{2.10}$$

and solve for β giving the optimal current angle β_{MTPA}

$$\frac{\partial T_e}{\partial \beta} = 0 \iff \beta_{MTPA} \approx \sin^{-1} \frac{-\psi_m + \sqrt{\psi_m^2 + 8(L_q - L_d)^2 I_s^2}}{4(L_q - L_d) I_s}\,. \tag{2.11}$$

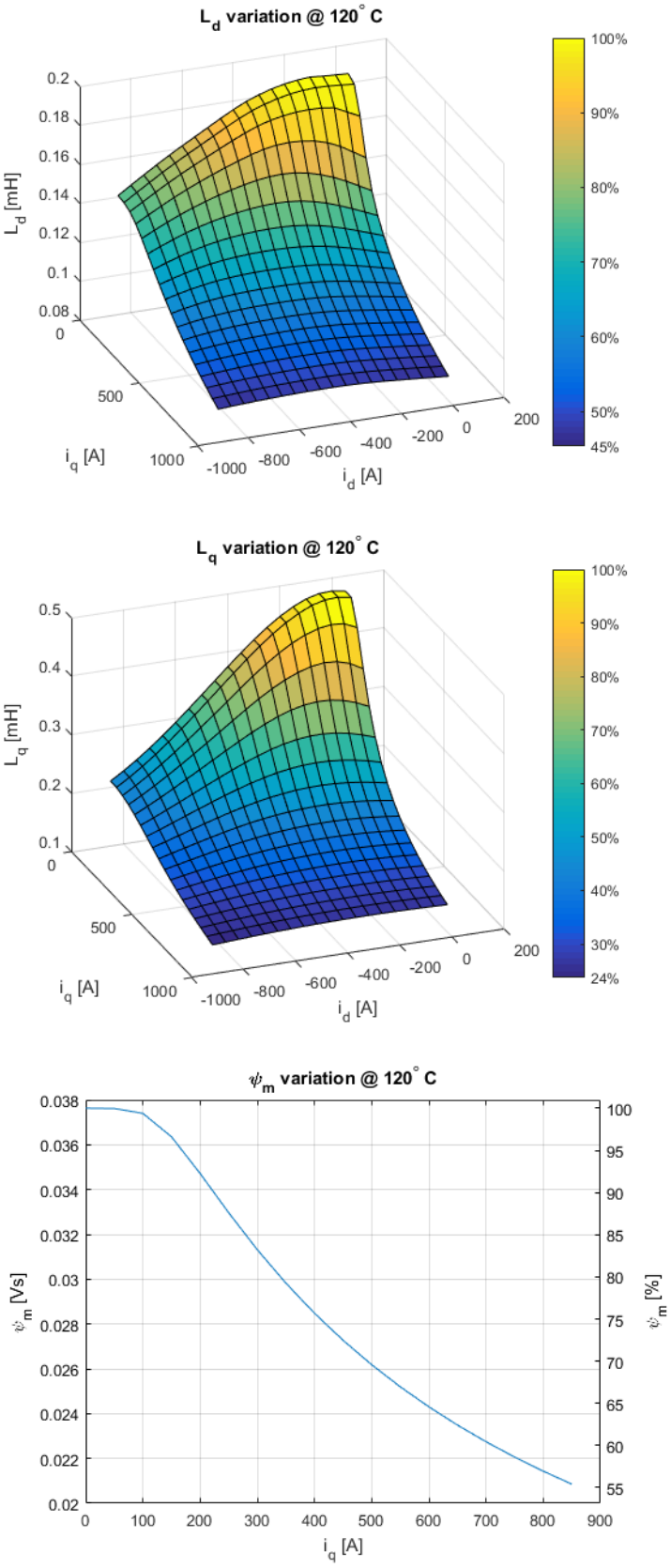

Figure 2.2: Visualization of the motor parameters' variation with respect to different i_d, i_q current levels. For the model ψ_m is assumed to only depend on the q-axis current.

Alternatively, (2.4) can be substituted into (2.10) to find the optimal i_d current as a function of i_q as

$$i_d = \frac{\psi_m}{2(L_q - L_d)} - \sqrt{\frac{\psi_m^2}{4(L_q - L_d)^2} + i_q^2}\,. \tag{2.12}$$

If the current relation (2.12) is substituted into (2.2), the result is a 4^{th} degree polynomial equation,

$$(L_q - L_d)^2 i_q^4 + \frac{2}{3p} T_e \psi_m i_q - \left(T_e \frac{2}{3p}\right)^2 = 0\,, \tag{2.13}$$

that can be used to calculate the i_q current from a given torque request. The obtained equations are used in the methods presented below.

2.4.1 Numerical methods combined with LuT

A common solution is to settle for an approximate solution of (2.13) using numerical techniques. In [14] and [15] the solution to the 4^{th} order equation (2.13) is solved with the Newton-Raphson iterative method. By using four iterative steps and selecting the initial conditions based on neglecting the high order term in (2.13), a good approximation can be found in real time. However for accurate solutions the author suggests that the method is combined with online estimated parameter or LuTs data which would solve the problem with varying motor parameters.

In [16] the numerical difficulties are instead handled through finding the current references from offline generated LuTs. The LuTs data are generated from torque measurements at different current angles at both high and low operating temperatures by considering the variation of the permanent magnet flux ψ_m. The current references are then found through linear interpolation between the LuTs data using an online permanent magnet flux observer. However the observer uses constant nominal motor parameters and hence an estimation error exists. In addition to this, the permanent magnet flux variation caused by temperature changes does not follow a linear pattern and hence an error is generated by the linear interpolation. Furthermore, generating the LuTs data also requires significant motor testing and therefore the method does not generalize well.

An alternative approach to handle the parameter variation is presented in [17] where the flux-linkage is modeled as a linear function of the stator currents. The method uses Finite Element Analysis (FEA) to approximate the magnetic saturation and cross-coupling effects on the flux-linkage. The linear flux-linkage model is combined with Levenberg-Marquardt numerical algorithm for accurate real time solutions of (2.13). The method shows promising results but the accuracy is highly depending on the precision in the FEA modelling which requires explicit knowledge about the structure of the IPMSM.

In [18] a fitting-based method of the flux-linkage is presented to overcome the inaccuracy caused by using the nominal motor parameters and avoid FEA modelling. The idea is to estimate 12 coefficients that can be used to calculate the flux-linkage from the measured d and q axis currents. The method uses measurement of

flux-linkage data at nine specific operating points in order to fit and estimates the coefficients using a minimum square technique offline. The estimated coefficients are then used from simplified online calculations of the optimal current reference. Although the method only requires a small number of data points, getting accurate flux-linkage measurements require advanced testing equipment compared to the common torque measurements.

In [19], in order to overcome the computationally heavy 4^{th} order equation, (2.12) is simplified using the Taylor series expansion for

$$\sqrt{1+x}\Big|_{x\approx 0} = 1 + \frac{1}{2}x - \frac{1}{8}x^2 + \mathcal{O}(x^3) \tag{2.14}$$

which, by discarding the x^2 term, results in the current relation

$$i_d = i_q^2 \frac{L_d - L_q}{\psi_m}\,, \tag{2.15}$$

which can be used to simplify the relation between the requested torque and i_q in (2.13).

Moreover, another local fitting method is used to model the IPMSM parameters based on current measurements for a number of specific reference points. The method ignores the effect of temperature changes, but the author suggests that the estimation process can be repeated for multiple operation conditions to increase robustness. However, this kind of LuT based approach still suffers the inaccuracies described above.

2.4.2 Signal Injection

A comparative analysis of various control algorithms for IPMSM, with focus on the ability to handle the effects from temperature variation, is presented in [6]. Apart from LuT based methods, the authors present adaptive techniques that are summarized in two categories, open loop extremum seeking control and closed loop torque controllers with online MTPA and parameter estimation.

For MTPA applications, extremum seeking control is commonly realized by an online-search based method called Signal Injection which was introduced in [20]. This technique is based on adjusting the current vector by injecting a small magnitude (A), high-frequency (w_h), sinusoidal variation on the current angle (β) given as

$$\beta^h = \beta + A\sin(w_h t), \tag{2.16}$$

which gives the current components

$$\begin{aligned} i_d^h &= I_s \cos\beta^h\,, \\ i_q^h &= I_s \sin\beta^h. \end{aligned} \tag{2.17}$$

Through the computation of the input power, based on the current and voltage measurement, the variation of the torque with respect to the change of the current angle could be analyzed.

Although injected-signal based methods have the advantage of being parameter independent, the convergence time to the MTPA point is too long to be used for online operations in fast-dynamical systems and additional copper losses are introduced.

2.4.3 Virtual Signal Injection

A similar technique to the one introduced in Section 2.4.2, Virtual Signal Injection (VSI) is introduced in [21]. The term *virtual* refers to the fact that no real signal is injected into the system hence avoiding the additional copper losses of the previous method. The injected signal is defined as in the previous method according to (2.16).

An advantage in using this method is that, differently from the non signal injected methods presented so far, the term T_d is not neglected, allowing a more accurate estimation of the MTPA, as presented in [9].

In order to estimate T_c, the Taylor expansion of the torque generated by the variation of the current angle is considered as

$$T_e(\beta + A\sin w_h t) = T_e(\beta) + \frac{\partial T_e}{\partial \beta} A \sin w_h t + \frac{\partial}{\partial \beta}\frac{\partial T_e}{\partial \beta} A^2 \sin w_h t^2 + \dots . \tag{2.18}$$

By considering the motor parameters to be piece-wise constant and by combining (2.1) and (2.2), it is possible to express T_e^h in function of the voltage, current and speed measurements as

$$T_e^h = \frac{3}{2p}\left(\frac{u_q - R_s i_q}{\omega} + \frac{u_d - R_s i_d}{i_q \omega} i_d^h\right) i_q^h . \tag{2.19}$$

By the use of a signal processing scheme, as presented in [9], T_c can be estimated. Combined with the use of LuTs of the motor parameters, a similar technique is used for the estimation of T_d, which will be described in more detail in Section 3.4.2. A controller is then used to generate a current reference that brings $\frac{\partial T_e}{\partial \beta}$ to zero in order to satisfy the MTPA condition (2.3).

Similarly to the Signal Injection method presented above, VSI has the advantage of being parameter independent. Due to the slow convergence to track the MTPA point, in [22] the VSI has been improved by using a square-wave current angle variation. On the other side, the use of LuTs for the estimation of T_d would increase the accuracy in the estimation of the MTPA trajectory only in the short term, hence it will not capture the variations of the parameters due to aging of the machine.

2.4.4 Adaptive methods

Within the adaptive closed loop control approaches, a few techniques are used in the literature. Among the more sophisticated methods, [23] and [24] present backstepping control approach that focuses on improving the reference tracking of an IPMSM. The IPMSM is described by a state space model taking the angular velocity and stator currents as states. The method uses a nonlinear disturbance observer to estimate the uncertainty in the state space model and achieves accurate torque tracking. Although the algorithm estimates the fully uncertain motor parameters

and demonstrates close to flawless parameter estimations in simulations, this method also lose accuracy by neglecting the term T_d in (2.5) [9].

A similar backstepping based control approach is also presented in [25]. In this paper the simplified MTPA relation (2.15) is utilized to simplify the controller design. A comprehensive Lyapunov function is constructed using the parameter error dynamics and the stability is proven using Barbalat's lemma. The results show accurate reference tracking and parameter estimation in simulation, but the performance of the MTPA tracking is not evaluated further.

A promising adaptive control approach in the form of MRAC combined with parameter estimation scheme is presented in [7] and further developed in [26] and [27]. The MRAC and parameter estimation used in these papers are described in detail in Section 3.2 and Subsection 3.3.1.

3
Control System

In this chapter the details behind the proposed control system is presented. In the first section an overview of the control system is shown to clarify how the sub parts are connected. The following sections aims to describe each part starting with the Internal Model Control (IMC) current controller, linear reference model and adaption blocks which makes up the main part of the MRAC. After that the parameter estimations and the use of current ripple measurements are described. The last section gives the details of the speed controller for the q-axis current reference and MTPA controller with VSI for the d-axis current reference.

3.1 Control System Overview

In order to clarify the connections between the subsystems that are presented below the schematic overview of the proposed control system that was shown in Section 1.2 is repeated in Figure 3.1.

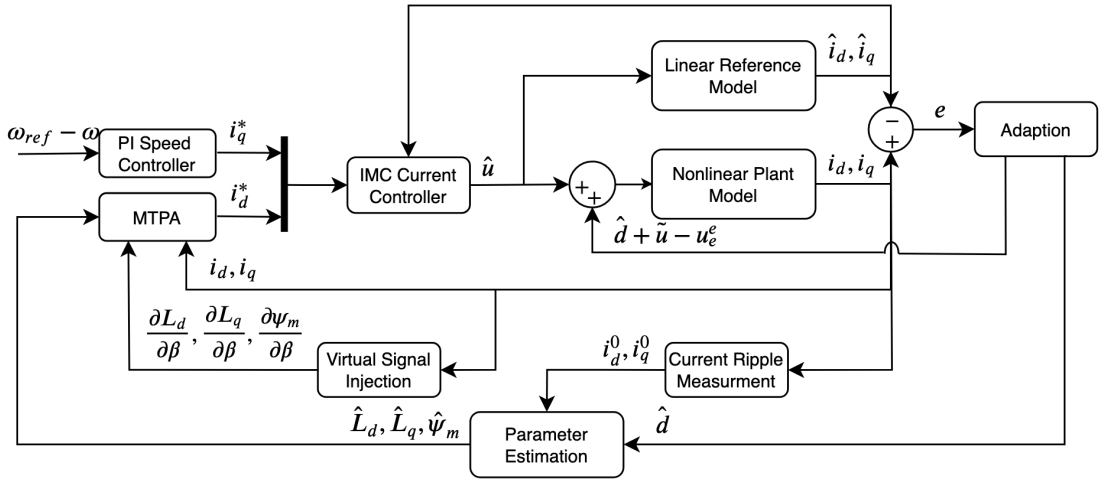

Figure 3.1: Overview of the proposed control system.

3.2 Model Reference Adaptive Control

For controlling the motor, an MRAC scheme inspired by the one presented in [7] is implemented. An overview of this scheme is presented in Figure 3.2. The idea

behind the control scheme is to induce a specified closed loop behaviour to the plant. In the control system, the desired control loop performance is described in terms of the dynamic characteristics of a reference model. The error signal $\boldsymbol{e}$ between the plant and the reference model output is then used to adjust the input to the plant through an adaption mechanism. MRAC is generally used for controlling systems with varying parameters as the controller is adapting to maintain the desired performance [28]. The following sections aim to describe each part of the control system in details.

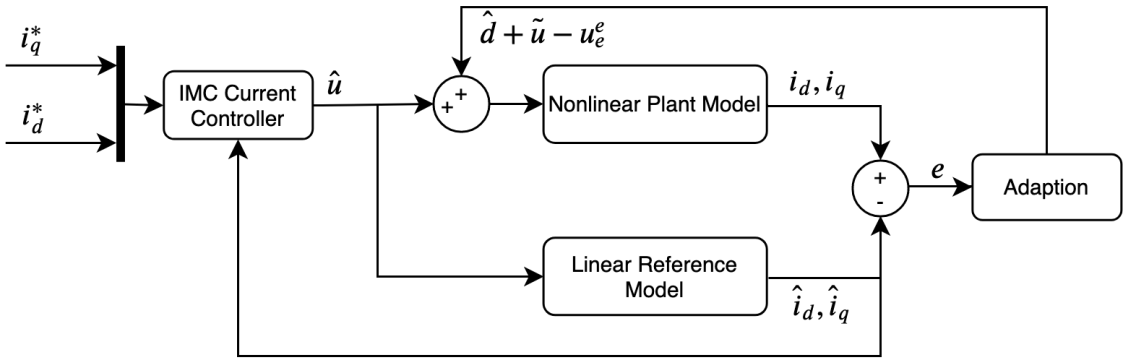

Figure 3.2: IPMSM Simulation model used to test the control system.

3.2.1 Reference model

For control purposes the motor model described in (2.1) is rewritten in a decoupled state space form

$$\begin{bmatrix} \dot{i}_d \\ \dot{i}_q \end{bmatrix} = \underbrace{\begin{bmatrix} -\frac{R_s}{L_d} & 0 \\ 0 & -\frac{R_s}{L_q} \end{bmatrix}}_{\boldsymbol{A}} \begin{bmatrix} i_d \\ i_q \end{bmatrix} + \underbrace{\begin{bmatrix} \frac{1}{L_d} & 0 \\ 0 & \frac{1}{L_q} \end{bmatrix}}_{\boldsymbol{B}} \left(\underbrace{\begin{bmatrix} u_d \\ u_q \end{bmatrix}}_{\boldsymbol{u_s}} + \underbrace{\begin{bmatrix} \omega L_q i_q \\ -\omega(L_d i_d + \psi_m) \end{bmatrix}}_{\boldsymbol{u_e}} \right), \tag{3.1}$$

where the matrices $\boldsymbol{A}$ and $\boldsymbol{B}$ are decoupled in the dq-axis and the coupled terms are collected in the additional input $\boldsymbol{u_e}$. By assuming that the true motor parameters are given by a constant nominal part along with a time dependent perturbation, the plant parameters can be expressed as

$$\begin{aligned} L_d(t) &= L_{d0} + \Delta L_d(t)\,, \\ L_q(t) &= L_{q0} + \Delta L_q(t)\,, \\ \psi_m(t) &= \psi_{m0} + \Delta \psi_m(t)\,, \\ R_s(t) &= R_{s0} + \Delta R_s(t)\,, \end{aligned} \tag{3.2}$$

where the subscript 0 denotes the nominal parameters and $\Delta L_d(t), \Delta L_d(t)$, $\Delta \psi_m(t)$ and $\Delta R_s(t)$ is the perturbation caused by, for example, the phenomena described in Section 2.3. Using the parameter description in (3.2), the reference model in state

space form can be expressed as

$$\begin{bmatrix}\dot{i}_d\\ \dot{i}_q\end{bmatrix} = \underbrace{\begin{bmatrix}-\frac{R_{s0}}{L_{d0}} & 0\\ 0 & -\frac{R_s 0}{L_{q0}}\end{bmatrix}}_{\boldsymbol{A_0}}\begin{bmatrix}i_d\\ i_q\end{bmatrix} + \underbrace{\begin{bmatrix}\frac{1}{L_{d0}} & 0\\ 0 & \frac{1}{L_{q0}}\end{bmatrix}}_{\boldsymbol{B_0}}\left(\underbrace{\begin{bmatrix}u_d\\ u_q\end{bmatrix}}_{\boldsymbol{u_s}} + \underbrace{\begin{bmatrix}\omega L_{q0} i_q\\ -\omega(L_{d0} i_d + \psi_{m0})\end{bmatrix}}_{\boldsymbol{u_e}} + \underbrace{\begin{bmatrix}d_d\\ d_q\end{bmatrix}}_{\boldsymbol{d}}\right), \tag{3.3}$$

where d is the total model error and disturbance decomposed in d- and q-axis components. Based on the voltage equilibrium (2.1) a detailed description of d is given as

$$\begin{aligned} d_d =& \Delta R_s i_d + \Delta L_d \frac{di_d}{dt} - \Delta L_q \omega i_q\,,\\ d_q =& \Delta R_s i_q + \Delta L_q \frac{di_q}{dt} + \left(\Delta L_d i_d + \Delta\psi_m\right).\omega \end{aligned} \tag{3.4}$$

Based on the state space form given in (3.3) a natural choice of reference model to use for the MRAC is obtained by neglecting the model error $\boldsymbol{d}$. Hence the reference model is defined by the state space

$$\begin{bmatrix}\dot{\hat{i}}_d\\ \dot{\hat{i}}_q\end{bmatrix} = \underbrace{\begin{bmatrix}-\frac{R_{s0}}{L_{d0}} & 0\\ 0 & -\frac{R_{s0}}{L_{q0}}\end{bmatrix}}_{\boldsymbol{A_0}}\begin{bmatrix}\hat{i}_d\\ \hat{i}_q\end{bmatrix} + \underbrace{\begin{bmatrix}\frac{1}{L_{d0}} & 0\\ 0 & \frac{1}{L_{q0}}\end{bmatrix}}_{\boldsymbol{B_0}}\left(\underbrace{\begin{bmatrix}\hat{u}_d\\ \hat{u}_q\end{bmatrix}}_{\hat{\boldsymbol{u}}} + \underbrace{\begin{bmatrix}\omega L_{q0}\hat{i}_q\\ -\omega(L_{d0}\hat{i}_d + \psi_{m0})\end{bmatrix}}_{\hat{\boldsymbol{u}}_{\boldsymbol{e}}}\right), \tag{3.5}$$

where the $\hat{\cdot}$ -symbol is used to denote the currents and voltages associated with the reference model.

3.2.2 Desired Dynamic Characteristic

Next step is to design the closed loop controller for the reference system and hence specify the desired dynamics. The controller is inspired by the IMC design method presented in [29] and aims to make the reference model behave like a low-pass filter,

$$\hat{\boldsymbol{i}} = \frac{\alpha}{s+\alpha}\boldsymbol{i}^*\,, \tag{3.6}$$

where s is the Laplace variable. To achieve this the controller is chosen as

$$\boldsymbol{C}(s) = \frac{\alpha}{s}\hat{\boldsymbol{G}}^{-1}(s)\,, \tag{3.7}$$

where $\hat{\boldsymbol{G}}(s)$ denotes the reference plant model. Note that this design is only possible for plants that have stable zeros. The closed loop transfer function becomes

$$\hat{\boldsymbol{G}}(s)\boldsymbol{C}(s)\left[\boldsymbol{I} + \hat{\boldsymbol{G}}(s)\boldsymbol{C}(s)\right]^{-1} = \frac{\frac{\alpha}{s}}{1+\frac{\alpha}{s}}\boldsymbol{I} = \frac{\alpha}{s+\alpha}\boldsymbol{I}\,, \tag{3.8}$$

where $\boldsymbol{I}$ is the identity matrix.

Using the state space matrices, $\boldsymbol{A_0}$ and $\boldsymbol{B_0}$, the controller $\boldsymbol{C}(s)$ is found as

$$\boldsymbol{C}(s) = \frac{\alpha}{s}\hat{\boldsymbol{G}}^{-1}(s) = \frac{\alpha}{s}\left((s\boldsymbol{I} - \boldsymbol{A_0})^{-1}\boldsymbol{B_0}\right)^{-1} = \frac{\alpha}{s}\boldsymbol{B_0}^{-1}(s\boldsymbol{I} - \boldsymbol{A_0})\,. \tag{3.9}$$

The reference model input voltage is thus given as

$$\hat{\boldsymbol{u}} = \alpha \boldsymbol{B_0}^{-1} \hat{\boldsymbol{e}} - \alpha \boldsymbol{B_0}^{-1} \boldsymbol{A_0} \int \hat{\boldsymbol{e}} dt - \hat{\boldsymbol{u}}_{\boldsymbol{e}} \,, \tag{3.10}$$

where $\hat{\boldsymbol{e}} = \boldsymbol{i}^* - \hat{\boldsymbol{i}}$ and $\hat{\boldsymbol{u}}_{\boldsymbol{e}}$ is added to directly cancel out the decoupled term $\hat{\boldsymbol{u}}_{\boldsymbol{e}}$ in (3.5). This structure has the advantage that only the parameter α needs to be determined. For a first order system α is related to the rise time t_r through the relation

$$t_r = \ln(9/\alpha), . \tag{3.11}$$

Hence the controller design is completed by selecting a desired rise time t_r.

3.2.3 Control Adaption Law

The reference model combined with the controller described in the previous section defines the desired closed loop performance. In order to ensure that the plant model achieves the desired behaviour, an adaptive control input is designed using Lyapunov theory to guarantee asymptotic convergence.

Using the state space description of the plant given in (3.3) and the reference model from (3.5), the current error dynamics between the two model currents can be calculated as

$$\dot{\boldsymbol{e}} = \dot{\boldsymbol{i}} - \dot{\hat{\boldsymbol{i}}} = \boldsymbol{A_0 e} + \boldsymbol{B_0}(\boldsymbol{u_s} - \hat{\boldsymbol{u}} + \boldsymbol{u_e^e} - \boldsymbol{d}) \,, \tag{3.12}$$

where u_e^e is the back-emf error

$$\boldsymbol{u_e^e} = \boldsymbol{u_e} - \hat{\boldsymbol{u}}_{\boldsymbol{e}} = \begin{bmatrix} \omega L_{q0} e_q \\ -\omega L_{d0} e_d \end{bmatrix} . \tag{3.13}$$

In order to stabilize the plant and force the model error to zero, the input $\boldsymbol{u_s}$ is selected as

$$\boldsymbol{u_s} = \tilde{\boldsymbol{u}} + \hat{\boldsymbol{u}} - \boldsymbol{u_e^e} + \hat{\boldsymbol{d}} \,, \tag{3.14}$$

where $\hat{\boldsymbol{d}}$ is the estimated model error $\boldsymbol{d}$. The error dynamics then take the following form

$$\dot{\boldsymbol{e}} = \boldsymbol{A_0 e} + \boldsymbol{B_0}(\tilde{\boldsymbol{u}} + \tilde{\boldsymbol{d}}) \,, \tag{3.15}$$

where $\tilde{\boldsymbol{d}}$ denotes the difference between the real and estimated model error, that is

$$\tilde{\boldsymbol{d}} = \hat{\boldsymbol{d}} - \boldsymbol{d} \,. \tag{3.16}$$

To ensure the stability of the plant, Lyapunov theory is used to design the adaption laws for $\tilde{\boldsymbol{u}}$ and $\tilde{\boldsymbol{d}}$. As the target is to ensure that both the current and plant model error converges to zero, a quadratic Lyapunov function is chosen as

$$V = \frac{1}{2}(\boldsymbol{e^T e} + \tilde{\boldsymbol{d}}^{\boldsymbol{T}} \boldsymbol{\Lambda} \tilde{\boldsymbol{d}}) \,, \tag{3.17}$$

where $\boldsymbol{\Lambda}$ is a control gain matrix chosen to be positive definite and diagonal in order to make the controller decoupled in the dq-axis. The derivative of (3.17) is found as

$$\dot{V} = \boldsymbol{e^T}(\boldsymbol{A_0 e} + \boldsymbol{B_0}\tilde{\boldsymbol{u}}) + \tilde{\boldsymbol{d}}^{\boldsymbol{T}}(\boldsymbol{B_0^T e} + \boldsymbol{\Lambda}\dot{\tilde{\boldsymbol{d}}}) \tag{3.18}$$

and the following adaption rules are chosen,

$$\tilde{\boldsymbol{u}} = -\boldsymbol{k}\boldsymbol{B}_{\boldsymbol{0}}^{\boldsymbol{T}}\boldsymbol{e}\,, \tag{3.19}$$

$$\tilde{\boldsymbol{d}} = -\boldsymbol{\Lambda}^{-\boldsymbol{1}}\boldsymbol{B}_{\boldsymbol{0}}^{\boldsymbol{T}}\int \boldsymbol{e}\,dt\,, \tag{3.20}$$

where $\boldsymbol{k}$ is a positive definite diagonal control gain matrix.

The resulting Lyapunov function derivative becomes

$$\dot{V} = \boldsymbol{e}^{\boldsymbol{T}}(\boldsymbol{A}_{\boldsymbol{0}} - \boldsymbol{B}_{\boldsymbol{0}}\boldsymbol{k}\boldsymbol{B}_{\boldsymbol{0}}^{\boldsymbol{T}})\boldsymbol{e} \leq 0\,, \tag{3.21}$$

where the inequality is obvious as $\boldsymbol{A}_{\boldsymbol{0}}$ is negative definite while $\boldsymbol{B}_{\boldsymbol{0}}$ is positive definite and hence equality can only be reached when $\boldsymbol{e} = \boldsymbol{0}$. From (3.15), (3.19) and (3.20) it is clear that $\boldsymbol{e} = \boldsymbol{0}$ implies that $\boldsymbol{d} = \boldsymbol{0}$. Therefore the system is globally asymptotically stable according to Lasalle's Invariance Principle [30].

3.2.4 Controller Gain Design

In order to choose the control gain matrices $\boldsymbol{\Lambda}$ and $\boldsymbol{k}$, the transient performance of the error signal is analyzed. Substituting the adaption laws (3.20) and (3.19), into the error dynamics in (3.15), and taking the derivative with respect to time yields

$$\ddot{\boldsymbol{e}} - (\boldsymbol{A}_{\boldsymbol{0}} - \boldsymbol{B}_{\boldsymbol{0}}\boldsymbol{k}\boldsymbol{B}_{\boldsymbol{0}}^{\boldsymbol{T}})\dot{\boldsymbol{e}} + \boldsymbol{B}_{\boldsymbol{0}}\boldsymbol{\Lambda}^{-\boldsymbol{1}}\boldsymbol{B}_{\boldsymbol{0}}^{\boldsymbol{T}}\boldsymbol{e} = \boldsymbol{0}\,. \tag{3.22}$$

As the system is decoupled in the dq-axis, the equation in each direction can be analyzed separately. For the d-axis the dynamics are described by

$$\ddot{e}_d + \left(\frac{R_0}{L_{d0}} + \frac{k_d}{L_{d0}^2}\right)\dot{e}_d + \frac{\Lambda_d}{L_{d0}^2}e_d = 0\,. \tag{3.23}$$

The controller gains can be determined by comparing the coefficients in (3.23) with the general second order system characteristic equation given as

$$s^2 + 2\zeta\omega_s s + \omega_s^2 = 0\,, \tag{3.24}$$

where ζ is the damping factor and $1/\omega_s$ is a second order time constant. Thus critical damping ($\zeta = 1$) is achieved by setting

$$\Lambda_d = \frac{1}{4}\left(R_0 + \frac{k_d}{L_{d0}}\right)^2\,. \tag{3.25}$$

The corresponding closed loop system has the form

$$G_d(s) = \frac{1}{(s+a)^2}\,, \tag{3.26}$$

where

$$a = \frac{1}{2L_{d0}}\left(R_0 + \frac{k_d}{L_{d0}}\right)\,. \tag{3.27}$$

The continuous transfer function is converted to discrete time using the corresponding z-transform

$$G_d(z) = T_s \frac{z e^{-aT_s}}{(z - e^{-aT_s})^2}\,, \tag{3.28}$$

where T_s is the sample time. The commonly used Euler forward discretization is accomplish by first order expansion of the Taylor series of the exponential terms yielding

$$G_d(z) = T_s \frac{z(1 - aT_s)}{(z - 1 + aT_s)^2}\,. \tag{3.29}$$

For discrete time stability the poles of the transfer function should be inside the unit circle, which gives the condition

$$-1 < aT_s - 1 < 1\,. \tag{3.30}$$

By substituting a from (3.27), results in the following condition for k_d

$$0 < \frac{T_s}{2L_{d0}} \left(R_0 + \frac{k_d}{L_{d0}} \right) < 2\,. \tag{3.31}$$

The same method is applied for the q-axis error dynamics which yields

$$\Lambda_q = \frac{1}{4} \left(R_0 + \frac{k_q}{L_{q0}} \right)^2 \tag{3.32}$$

and

$$0 < \frac{T_s}{2L_{q0}} \left(R_0 + \frac{k_q}{L_{q0}} \right) < 2\,. \tag{3.33}$$

Hence the control parameter matrix $\boldsymbol{\Lambda}$ is fully determined by (3.25) and (3.32) and $\boldsymbol{k}$ can be selected based on the conditions in (3.31) and (3.33).

3.2.5 Estimating the model error

From the adaption law presented in (3.20) the value of $\tilde{\boldsymbol{d}} = \hat{\boldsymbol{d}} - \boldsymbol{d}$ is obtained. However in order to provide the desired input to the system ($\boldsymbol{u_s}$), according to (3.14), an accurate estimation of the model error $\hat{\boldsymbol{d}}$ is required. In order to estimate $\hat{\boldsymbol{d}}$ the dynamics of $\tilde{\boldsymbol{d}}$ is studied by inserting the adaption laws (3.19) and (3.20) into the model error dynamics in (3.15),

$$\boldsymbol{d} = \boldsymbol{B_0}^{-T} \boldsymbol{\Lambda} \boldsymbol{B_0}^{-1} \ddot{\tilde{\boldsymbol{d}}} - (\boldsymbol{A_0} - \boldsymbol{k} \boldsymbol{B_0}^T \boldsymbol{B_0}) \boldsymbol{\Lambda} \boldsymbol{B_0}^{-T} \boldsymbol{B_0}^{-1} \dot{\tilde{\boldsymbol{d}}} + \hat{\boldsymbol{d}}\,. \tag{3.34}$$

Because of the choice of state space model and gain matrices, (3.34) is decoupled in the dq-axis. By defining the two time constants,

$$\begin{aligned} \boldsymbol{T_m} &= \boldsymbol{B_0}^{-T} \boldsymbol{\Lambda} \boldsymbol{B_0}^{-1} (\boldsymbol{B_0}^T \boldsymbol{k} \boldsymbol{B_0} - \boldsymbol{A_0})\,, \\ \boldsymbol{T_\sigma} &= (\boldsymbol{B_0}^T \boldsymbol{k} \boldsymbol{B_0} - \boldsymbol{A_0})\,, \end{aligned} \tag{3.35}$$

the error dynamics can be rewritten into the general form

$$\boldsymbol{d} = \tilde{\boldsymbol{d}} (\boldsymbol{T_m} s (\boldsymbol{T_\sigma} s + \boldsymbol{I})) + \hat{\boldsymbol{d}}\,. \tag{3.36}$$

The relation (3.36) can be seen as a closed loop system where the plant uncertainty is treated as an additive disturbance signal, see Figure 3.3. The reference input is selected to zero as the target is to generate the input $\hat{\boldsymbol{d}}$ such that the model error $\tilde{\boldsymbol{d}}$ converges to zero.

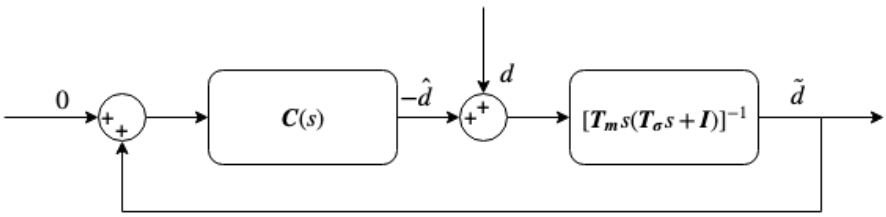

Figure 3.3: Equivalent closed-loop system for the model error dynamics.

In order to achieve the reference, a Symmetrical Optimum PI-controller is implemented. Let the PI controller transfer function be given by

$$\boldsymbol{C}(s) = (\boldsymbol{I} + \boldsymbol{T_n} s)(\boldsymbol{T_i} s)^{-1}\,, \tag{3.37}$$

where $\boldsymbol{T_i}$ and $\boldsymbol{T_n}$ are diagonal matrices because of the decoupled property.

The objective of Symmetrical Optimum design is to force the magnitude of the closed-loop transfer function close to one for a wide range of low frequency inputs

$$|\boldsymbol{T}(j\omega)|\Big|_{\omega<\omega 0} \approx \boldsymbol{I}\,. \tag{3.38}$$

This is done by studying the closed loop dynamics in the frequency domain

$$\boldsymbol{T}(s) = \boldsymbol{C}(j\omega)\boldsymbol{G}(j\omega)\left[\boldsymbol{I} + \boldsymbol{C}(j\omega)\boldsymbol{G}(j\omega)\right]^{-1}\,. \tag{3.39}$$

As the system is decoupled, the d and q-axis dynamics can be considered separately. However, in order to keep the notation simple, the $\cdot_d$ subscript is omitted in the following equations. Therefore, (3.39) for the d-axis can be expressed as

$$T(s) = \frac{1 + T_n s}{T_i T_m T_\sigma s^3 + T_d T_m s^2 + T_n s + 1}\,. \tag{3.40}$$

Setting $s = j\omega$, the magnitude of (3.40) becomes

$$|T(j\omega)| = \sqrt{\frac{1 + \omega^2 T_n^2}{(1 - T_i T_m \omega^2)^2 + \omega^2 (T_n - T_i T_m T_p \omega^2)^2}}\,. \tag{3.41}$$

Expanding the denominator in (3.41) yields

$$D(j\omega) = (T_i T_m T_\sigma)^2 \omega^6 + T_i T_m (T_i T_m - 2T_n T_\sigma)\omega^4 + [T_n^2 - 2T_i T_m]\omega^2 + 1\,. \tag{3.42}$$

For Symmetry Optimum controller design the gains should be chosen such that the terms of ω^4 and ω^2 evaluates to zero, resulting in the conditions

$$\begin{aligned} T_i T_m &= 2T_n T_\sigma\,, \\ T_n^2 &= 2T_i T_m\,. \end{aligned} \tag{3.43}$$

From the equation system (3.43) the PI-controller parameters are found as

$$T_n = 4T_\sigma \,, \tag{3.44}$$

$$T_i = 8\frac{T_\sigma^2}{T_m} \,. \tag{3.45}$$

A similar analysis can be done for the q-axis resulting in the final controller

$$\boldsymbol{C}(s) = \frac{1}{2}\boldsymbol{T_m}\boldsymbol{T_\sigma}^{-1}\tilde{\boldsymbol{d}} + \frac{1}{8}\boldsymbol{T_m}(\boldsymbol{T_\sigma}^{-1})^2 \int \tilde{\boldsymbol{d}} dt \,. \tag{3.46}$$

The controller is hence completely determined based on the plant model and previous controller gains $\boldsymbol{k}$ and $\boldsymbol{\Lambda}$.

3.3 Parameter Estimation

This section describes the derivation of the equations needed in order to estimate the motor parameters.

3.3.1 Estimated Model Error

From the MRAC scheme deployed in the previous section, an estimation of the difference $\hat{\boldsymbol{d}}$ between the plant and the reference model is obtained. Using the detailed expression of the model error given in (3.4), it can be assumed that

$$\begin{aligned} \hat{d}_d &= \Delta R_s i_d + \Delta L_d \frac{di_d}{dt} - \Delta L_q \omega i_q \,, \\ \hat{d}_q &= \Delta R_s i_q + \Delta L_q \frac{di_q}{dt} + (\Delta L_d i_d + \Delta\psi_m)\omega \,. \end{aligned} \tag{3.47}$$

For digital implementation, the derivatives are estimated using first order Euler approximation with sample time t_{est}. The estimated model error (3.47) can be expressed as a system linear in the motor parameter as

$$\begin{bmatrix} \hat{d}_d(n) \\ \hat{d}_q(n) \end{bmatrix} = \begin{bmatrix} \frac{i_d(n)-i_d(n-1)}{t_{est}} & \omega i_q(n) & 0 & i_d(n) \\ \omega i_d(n) & \frac{i_q(n)-i_q(n-1)}{t_{est}} & \omega & i_q(n) \end{bmatrix} \begin{bmatrix} \Delta L_d \\ \Delta L_q \\ \Delta\psi_m \\ \Delta R_s \end{bmatrix} , \tag{3.48}$$

where n denotes the discrete time step.

However as four parameters need to be estimated, the linear system in (3.48) must be supplemented with two additional equations. The problem is solved using the information contained in the current ripple as presented in the following section.

3.3.2 Current Ripple Modelling

In order to integrate (3.48) with two additional equations, the stator current ripple model presented in [8] is used. The idea is to use several measurement points for

the current and voltage within each switching cycle of the inverter to observe an additional transient state caused by the stator current ripple.

Since the system is supplied by a three-phase current, the dominating ripple frequency component will be of three times the fundamental frequency [8]. The current ripple in the dq-axis, ignoring higher order harmonics of the switching frequency, are thus given by

$$\begin{aligned} i_{d,ripple} &= -A_d \cos(3\theta_v - \varphi_d)\,, \\ i_{q,ripple} &= A_q \sin(3\theta_v - \varphi_q)\,, \end{aligned} \tag{3.49}$$

where A_d, A_q are the ripple amplitude, θ_v is the voltage vector angle and φ_d, φ_q are the phase delays of the d- and q-axis current components. Notice that the voltage angle vector is separated from the electrical angle θ and can be estimated as

$$\theta_v = \theta + \arctan \frac{u_q}{u_d}\,. \tag{3.50}$$

Using the switching pattern of the inverter, as seen in Figure 3.4, the current ripple can be modeled as

$$\begin{aligned} i_{d,ripple} &= \Delta I_{d,0} + \Delta I_{d,1}\,, \\ i_{q,ripple} &= \Delta I_{q,0} + \Delta I_{q,1}\,, \end{aligned} \tag{3.51}$$

where $\Delta I_{d(q),0}$ and $\Delta I_{d(q),1}$ are the current variations within switching section 0 and 1 respectively, as seen in Figure 3.4. S_A, S_B and S_C are the relay switching states of the three phases a, b and c.

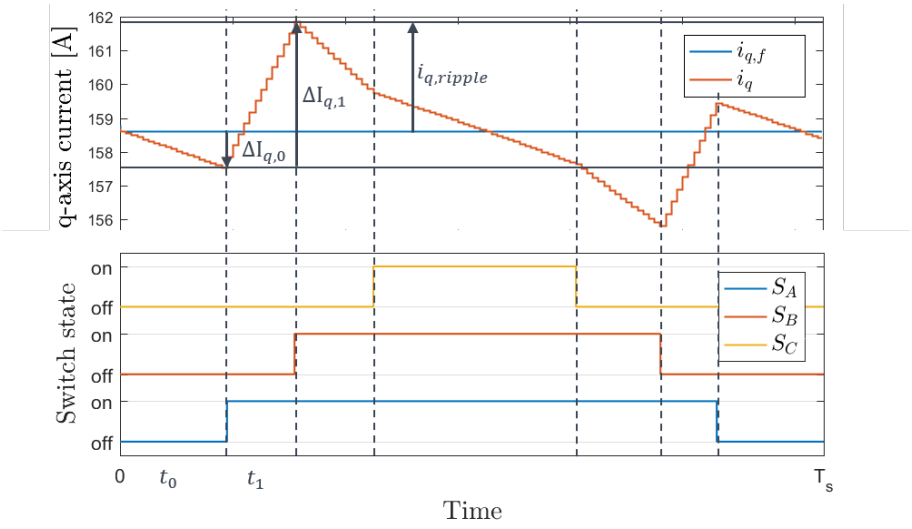

Figure 3.4: Inverters' switching pattern and the corresponding current ripple dynamics.

By using the motor model (2.1), these current variations can be calculated as

$$\begin{aligned} \Delta I_{d,i} &= t_i \dot{i}_{d,i} = \frac{t_i}{L_d}\left(-R_s i_{d,f} + \omega L_q i_{q,f} + u_{d,i}\right)\,, \\ \Delta I_{q,i} &= t_i \dot{i}_{q,i} = \frac{t_i}{L_q}\left(-R_s i_{q,f} - \omega(L_q i_{d,f} + \psi_m) + u_{q,i}\right)\,, \end{aligned} \tag{3.52}$$

where $i_{d,f}$ and $i_{q,f}$ is the fundamental current components, t_i and $u_{d,i}$ are the switching time and input voltage at switching section i. As the mechanical dynamics is much slower than the electrical, the rotational speed ω is assumed to be constant within a switching period. Substituting the current variation expressions in (3.52) into (3.51), the current ripple is modeled as

$$\begin{aligned} i_{d,ripple} &= \left(\frac{u_{d,0}t_0 + u_{d,1}t_1}{t_0 + t_1} + \omega L_q i_{q,f} - R_s i_{d,f} \right) \frac{t_0 + t_1}{L_d} , \\ i_{q,ripple} &= \left(\frac{u_{q,0}t_0 + u_{q,1}t_1}{t_0 + t_1} + \omega (L_d i_{d,f} + \psi_m) - R_s i_{q,f} \right) \frac{t_0 + t_1}{L_q} . \end{aligned} \tag{3.53}$$

Thus, if the current ripple can be estimated, (3.53) can be used to estimate the motor parameters.

According to (3.51), the current ripples can be calculated from the current measured at the end of switching section 1 subtracted by the measurement at the start of switching section 0. As the measurements contain additional zero-mean white noise from current sensors and harmonic components, the detailed description of the acquired measurement is given by

$$i^m_{d(q),ripple} = i_{d(q),ripple} + w + a_0 + \sum_{n=1, n\neq 3} a_n \sin\left(n\theta_v + \varphi_n\right) , \tag{3.54}$$

where $i^m_{d(q),ripple}$ is the current ripple measurement, w is white noise, a_0 is the DC component and the sum represents the harmonic components. In order to extract the current ripple components ($i_{d(q),ripple}$), the d- and q-axis measurement is multiplied with $-\cos 3\theta_v$ and $\sin 3\theta_v$ respectively resulting in

$$\begin{aligned} i^h_d =& \frac{A_d}{2} \left(\cos\varphi_d + \cos\left(6\theta_v - \varphi_d\right)\right) - \left(w + a_0\right)\cos 3\theta_v + \\ & - \sum_{n=1, n\neq 3} \frac{a_n}{2} \left(\sin\left[(n+3)\theta_v + \varphi_n\right] + \sin\left[(n-3)\theta_v + \varphi_n\right]\right) , \\ i^h_q =& \frac{A_q}{2} \left(\cos\varphi_q - \cos\left(6\theta_v - \varphi_q\right)\right) - \left(w + a_0\right)\sin 3\theta_v + \\ & - \sum_{n=1, n\neq 3} \frac{a_n}{2} \left(\cos\left[(n+3)\theta_v + \varphi_n\right] - \cos\left[(n-3)\theta_v + \varphi_n\right]\right) . \end{aligned} \tag{3.55}$$

By using a low-pass filter and multiplying the output with a factor two, the DC component is obtained as

$$\begin{aligned} i^0_d =& A_d \cos\varphi_d = i_{d,ripple}\Big|_{\theta_v = \frac{1}{3}\pi, \pi, \frac{5}{3}\pi} , \\ i^0_q =& A_q \cos\varphi_q = i_{q,ripple}\Big|_{\theta_v = \frac{1}{6}\pi, \frac{5}{6}\pi, \frac{3}{2}\pi} , \end{aligned} \tag{3.56}$$

where the last equality is obtained from (3.49). In order to remove the fundamental and harmonic components of the current measurement, the cut-off frequency w_c for the low-pass filter should be selected to be less than half the fundamental frequency. The fundamental frequency is approximately given by the electrical rotation speed

(ω), see (3.50), as the relation between the input voltages (u_d and u_q) are chaining much slower than the electrical angle (θ). Simultaneously, a high cut-off frequency is needed to capture the rapid changes in stator current ripple, hence an adaptive cutoff frequency as a function of the rotation speed is used according to

$$w_c = \max(k_c\omega, w_{c,min}) \,, \tag{3.57}$$

where $k_c < 0.5$ and $w_{c,min}$ is a minimum value for the cut-off frequency at low speed.

By using (3.56) and given that the measurements are done at specific voltage vector angles, the current ripple model (3.53) can be expressed as

$$\begin{aligned} i_d^0 =& (\frac{u_{d,0}t_0 + u_{d,1}t_1}{t_0 + t_1} + \omega L_q i_{q,f} - R_s i_{d,f}) \frac{t_0 + t_1}{L_d}\bigg|_{\theta_v = \frac{1}{3}\pi, \pi, \frac{5}{3}\pi} \,, \\ i_q^0 =& (\frac{u_{q,0}t_0 + u_{q,1}t_1}{t_0 + t_1} - \omega(L_d i_{d,f} + \psi_m) - R_s i_{q,f}) \frac{t_0 + t_1}{L_q}\bigg|_{\theta_v = \frac{1}{6}\pi, \frac{5}{6}\pi, \frac{3}{2}\pi} \,. \end{aligned} \tag{3.58}$$

In order to combine the current ripple equations with the model error given in (3.47), the contribution from the nominal parameters ($R_{s0}, L_{d0}, L_{q0}\psi_{m0}$) needs to be subtracted. By defining

$$\begin{aligned} \Delta u_d =& \frac{u_{d,0}t_0 + u_{d,1}t_1}{t_0 + t_1} + \omega L_{q0} i_{q,f} - R_0 i_{d,f} - \frac{L_{d0} i_d^0}{t_0 + t_1}\bigg|_{\theta_v = \frac{1}{3}\pi, \pi, \frac{5}{3}\pi} \,, \\ \Delta u_q =& \frac{u_{q,0}t_0 + u_{q,1}t_1}{t_0 + t_1} - \omega(L_{d0} i_{d,f} + \psi_{m0}) - R_0 i_{q,f} - \frac{L_{q0} i_q^0}{t_0 + t_1}\bigg|_{\theta_v = \frac{1}{6}\pi, \frac{5}{6}\pi, \frac{3}{2}\pi} \,, \end{aligned} \tag{3.59}$$

the system in (3.48) can be expanded as

$$\begin{bmatrix} \hat{d}_d(n) \\ \hat{d}_q(n) \\ \Delta u_d(n) \\ \Delta u_q(n) \end{bmatrix} = \begin{bmatrix} \frac{i_{d,f}(n) - i_{d,f}(n-1)}{t_{est}} & \omega i_{q,f}(n) & 0 & i_{d,f}(n) \\ \omega i_{d,f}(n) & \frac{i_{q,f}(n) - i_{q,f}(n-1)}{t_{est}} & \omega & i_{q,f}(n) \\ \frac{i_d^0}{t_0 + t_1} & -\omega i_{q,f} & 0 & i_{d,f} \\ \omega i_{d,f}(n) & \frac{i_q^0(n)}{t_0 + t_1} & \omega & i_{q,f}(n) \end{bmatrix} \begin{bmatrix} \Delta L_d \\ \Delta L_q \\ \Delta \psi_m \\ \Delta R_s \end{bmatrix} \,, \tag{3.60}$$

where the subscript $\cdot_f$ is added in the first two equations to emphasize that the model error uses the fundamental current component.

As the simulation motor model that is used to test the control system assumes R_s as constant, see the details in Section 4.1, the system of equations needed to estimate the resulting parameters can be expressed as

$$\underbrace{\begin{bmatrix} \hat{d}_d(n) \\ \hat{d}_q(n) \\ \Delta u_d(n) \end{bmatrix}}_{\boldsymbol{y}} = \underbrace{\begin{bmatrix} \frac{i_{d,f}(n) - i_{d,f}(n-1)}{t_{est}} & \omega i_{q,f}(n) & 0 \\ \omega i_{d,f}(n) & \frac{i_{q,f}(n) - i_{q,f}(n-1)}{t_{est}} & \omega \\ \frac{i_d^0(n)}{t_0 + t_1} & -\omega i_{q,f}(n) & 0 \end{bmatrix}}_{\boldsymbol{\varphi}} \underbrace{\begin{bmatrix} \Delta L_d \\ \Delta L_q \\ \Delta \psi_m \end{bmatrix}}_{\boldsymbol{\theta}} \,, \tag{3.61}$$

where the third row of $\boldsymbol{\varphi}$ is updated at $\theta_v = \frac{1}{3}\pi, \pi, \frac{5}{3}\pi$.

3.3.3 Recursive Least Squares

The system obtained in (3.61) is linear in the motor parameter variations ($\boldsymbol{\theta}$), and is given in the form

$$\boldsymbol{y}(t) = \boldsymbol{\varphi(t)\theta(t)}\,, \tag{3.62}$$

which can be solved with a standard Recursive Least Squares (RLS) algorithm. More details on the RLS algorithm are treated in Appendix B. To maintain estimation stability through the entire operation region, the RLS algorithm is stopped when the motor speed ω or the i_d and i_q currents amplitudes are close to zero in order to prevent high condition numbers for $\boldsymbol{\varphi}$.

Using the equation system (3.60), the method could be generalized to estimate all four parameters at the cost of higher computational load.

3.4 Current references and MTPA

This section describes how the current references are derived in order to satisfy the MTPA relation (2.5).

3.4.1 Speed control and q-axis reference current

A Proportional Integral (PI) controller is used to control the motor speed and generate a reference for the q-axis current as

$$i_q^*(n) = \left(K_{p,q} + K_{i,q}(1 + di_q^*(n))\frac{T_{q,s}}{z-1}\right) e_\omega(n)\,, \tag{3.63}$$

where $K_{p,q}, K_{i,q}$ are the proportional and integral gain respectively, $e_\omega(n)$ is the error between the reference and the measured motor speed, $T_{q,s}$ is the time constant, $di_q^*(n)$ is the difference between the saturated and unsaturated output and acts as an anti-windup.

3.4.2 Virtual Signal Injection and d-axis reference current

In order to generate the d-axis reference i_d^* and achieve MTPA operations for the motor, the MTPA equation (2.5) is used. The T_c term given in (2.6) is calculated using the measured i_d, i_q currents along with the estimated parameters according to

$$\hat{T}_c = \frac{3}{2}p\left[\hat{\psi}_m i_d + (\hat{L}_d - \hat{L}_q)(i_d^2 - i_q^2)\right]\,. \tag{3.64}$$

For the second term T_d, the derivatives of the parameters with respect to the current angle β are required. These are estimated with an VSI technique inspired by the one used in [9]. The parameter variations are estimated using the LuT data shown in section 2.3. From the measured dq-axis currents, the current magnitude and angle are calculated as

$$\begin{aligned} I_s &= \sqrt{i_d^2 + i_q^2}\,, \\ \beta &= \arctan\frac{i_q}{i_d}\,. \end{aligned} \tag{3.65}$$

A small sinusoidal perturbation is then added to the current angle

$$\beta^h = \beta + A\sin(\omega_h t)\,, \tag{3.66}$$

where ω_h is the angular frequency of the injected signal. The resulting dq-currents

$$\begin{aligned} i_d^h =& I_s \cos\beta^h\,, \\ i_q^h =& I_s \sin\beta^h\,, \end{aligned} \tag{3.67}$$

are given as inputs to the LuTs generating the parameters. Using Taylor series expansion, the obtained parameter, here shown for ψ_m, can be expanded as

$$\begin{aligned} \psi_m^h =& \psi_m(\beta + A\sin(\omega_h t)) = \\ =& \psi_m(\beta) + \frac{\partial\psi_m}{\partial\beta} A\sin(\omega_h t) + \frac{1}{2}\frac{\partial^2\psi_m}{\partial\beta^2} A^2\sin^2(\omega_h t) + \mathcal{O}(A^3)\,. \end{aligned} \tag{3.68}$$

The term containing the derivative of $\partial\psi_m/\partial\beta$ can thus be extracted using a band-pass filter centered around the injected frequency ω_h. The output from the band-pass filter is then multiplied with the injected sinusoidal such that

$$\frac{\partial\psi_m}{\partial\beta} A\sin(\omega_h t)\sin(\omega_h t) = \frac{\partial\psi_m}{\partial\beta} A\frac{1}{2}(1-\cos(2\omega_h t))\,. \tag{3.69}$$

With the help of a low-pass filter, the constant part is extracted and multiplied with the gain $2/A$ to obtain the parameter derivative. The whole signal processing is summarized in Figure 3.5. The same technique is used to estimate the derivatives of the other parameters such that

$$\hat{T}_d = \frac{3}{2}p\left[\widehat{\frac{\partial\psi_m}{\partial\beta}} i_q + \widehat{\frac{\partial L_d}{\partial\beta}} i_d i_q - \widehat{\frac{\partial L_q}{\partial\beta}} i_d i_q\right]\,, \tag{3.70}$$

can be calculated using the measured currents.

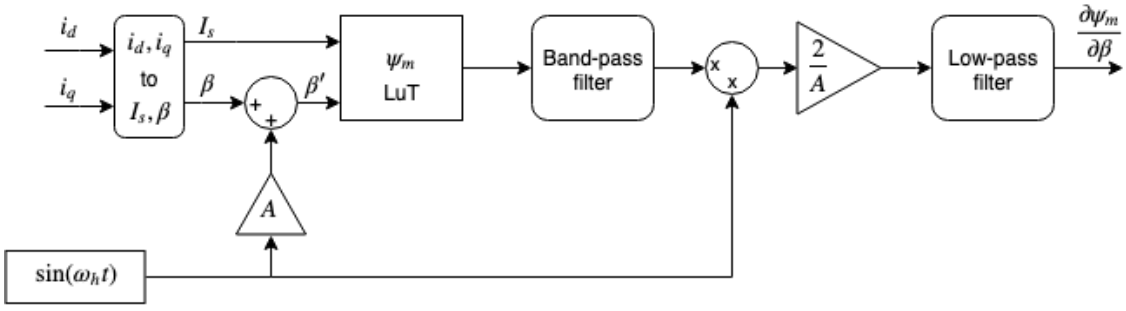

Figure 3.5: Signal processing to obtain the derivative of the parameters with respect to β, here shown for ψ_m.

The total expression for the torque derivative is forced to zero using a PI controller that generates the i_d^*. Thus the error signal is formed as

$$e_{MTPA} = 0 - \left(\hat{T}_c(n) + \hat{T}_d(n)\right)\,. \tag{3.71}$$

Based on the error signal the PI controller for generating the d-axis current reference is obtained as

$$i_d^*(n) = \left(K_{p,d} + K_{i,d}(1 + di_d^*(n)) \frac{T_{d,s}}{z-1} \right) e_{MTPA}\,, \tag{3.72}$$

where $K_{d,p}, K_{d,i}$ are the proportional and integral gain respectively, $T_{d,s}$ is the time constant and $di_q^*(n)$ is the difference between the saturated and unsaturated output and acts as an anti-windup.

4
Evaluation Methods

In this chapter the methods used to evaluate the control system are presented. In the first section, the characteristics of the motor model used in simulation is presented. The following section describes how the true MTPA curve of the motor model is derived, that will be used as benchmark to evaluate the algorithm. After that, the details of the default Hybrid Kit algorithm, that CEVT is currently evaluating, is presented. The algorithm will be used as a baseline for comparison with the proposed algorithm. Finally, the test scenarios used to evaluate the algorithms are described.

4.1 IPMSM simulation model

For evaluating the performance of the control systems, an IPMSM model is developed in Simulink. The complete model consists of a Power Electronics (PE) model along with a model of the dynamics of the motor.

For the PE model to work, the input u is converted to the abc-frame where Sinusoidal Pulse Width Modulation is used to determine the switching instants for the power transistors, for details see [31]. The details of the Parks- Clarke transformation are found in Appendix A. The resulting voltages are then transformed back to the dq-frame and given as inputs to the motor model.

To accurately represent the real system, the motor parameters used in the model are implemented as nonlinear functions of the stator currents using LuTs, as presented in Section 2.3. The winding resistance R_s is set constant to 0.16 Ω. The motor is modeled in the dq-frame using the relations presented in (2.1) and (2.2) to obtain the stator currents and produced torque. The electrical angular velocity along with the rotor angular position are then calculated as

$$\omega = \frac{N_p}{2} \int \frac{T_e - T_L}{J} dt \tag{4.1}$$

and

$$\theta = \int \omega dt \,, \tag{4.2}$$

where N_p is the number of pole pairs, T_L is the total load torque and J is the rotor inertia. An overview of the complete motor model is shown in Figure 4.1.

The motor model is expected to represent the complexity of a real IPMSM as the parameters vary non-linearly with the currents based on the LuT data. To further represent a real system all measurements from the motor model are assumed to be affected by noise. The sensor noise is modeled as zero-mean band limited white

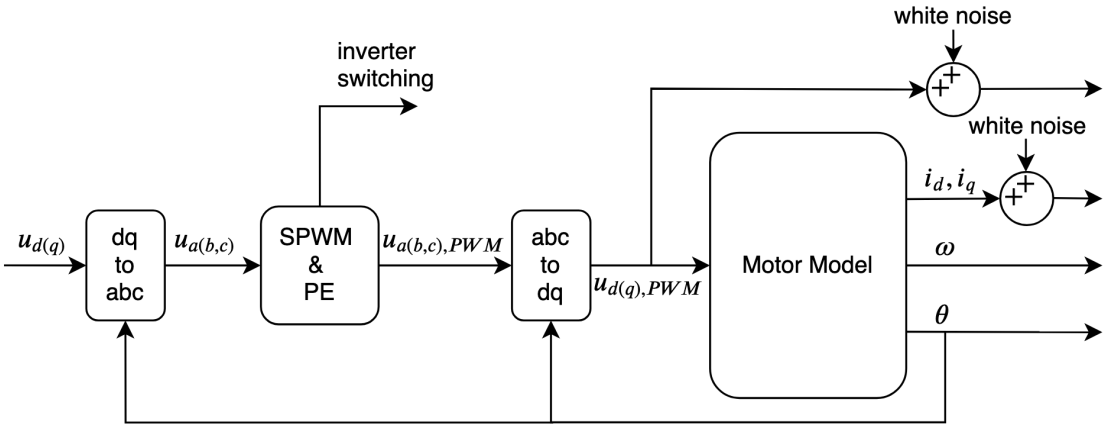

Figure 4.1: IPMSM simulation model used to evaluate the control system.

noise with peak amplitudes corresponding to 0.2 % of the maximum output of each sensor, as done in [8].

As the proposed control system is developed to work without any prior knowledge of the motor parameters[1], it is assumed that only taking the parameter variations caused by inductance saturation with different current levels should be sufficient to validate the functionality of the control system. That is, if the system is able to track the fast changes caused by inductance saturation, the slow changes caused by temperature variations and aging should be handled as well.

4.2 Identifying the true MTPA curve

In order to validate the performance of the control system, the true MTPA curve needs to be identified.

The motor model provided by CEVT is a nonlinear machine model as described in Section 4.1. Since making a complete torque map for the motor model would be rather time consuming, the true MTPA curve will instead be estimated through a curve fitting method, similar to what was done in [32]. The method can be summarized in the following steps:

1. Select a constant torque reference: $T_e^* = const$
2. Measure output current for a span of current angles β in a region close to the optimal operation point
3. Identify the MTPA point for the given torque reference based on the minimum amplitude of the current
4. Repeat the previous steps for a number of different torque levels
5. Interpolate a function between the estimated MTPA points to estimate the MTPA trajectory

The procedure is performed using a PI controller and measuring the currents after the model reaches steady state at each current angle. In Figure 4.2 the true

[1]Except for the LuTs used in the virtual signal injection, as described in Section 3.4.2. Updating these LuT over time with the help of the parameter estimations is suggested as a future work, see Section 7.1.

MTPA trajectory for a constant speed of 300 rad/s can be seen.

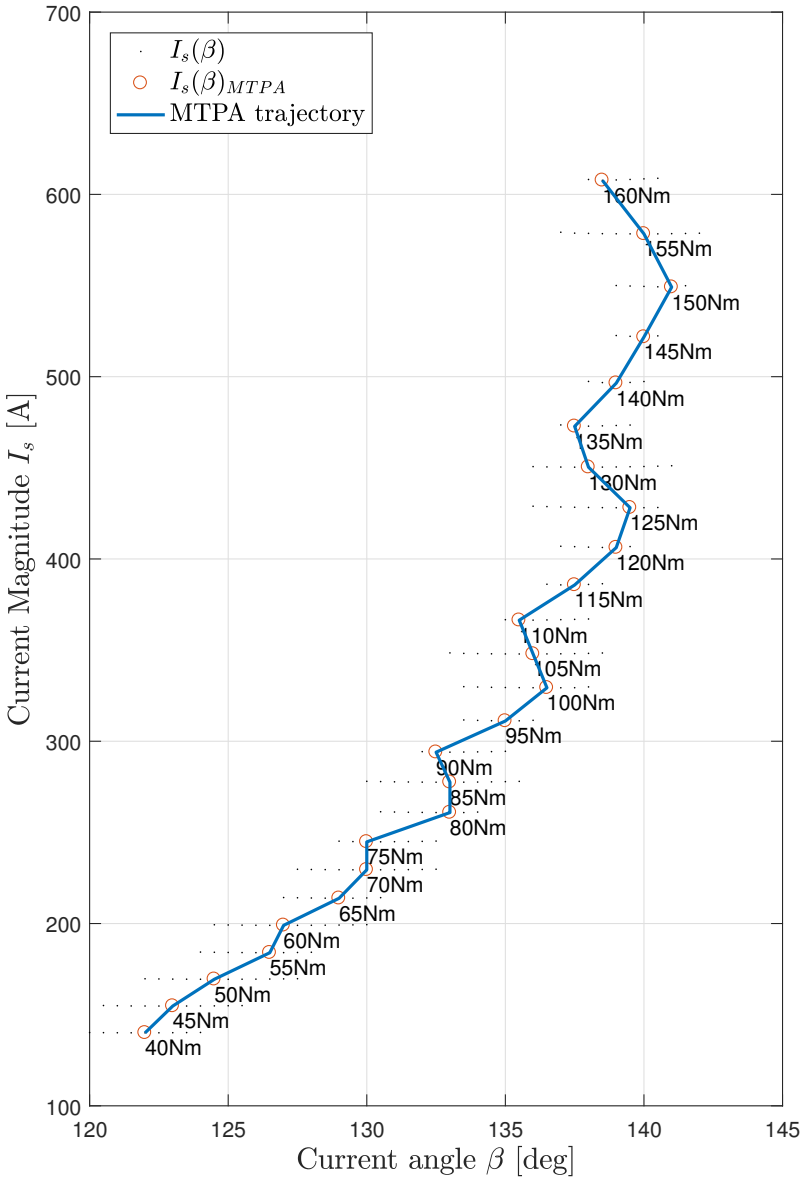

Figure 4.2: Identified true MTPA trajectory for the motor model.

4.3 Hybrid Kit algorithm

As mentioned in Section 1.1, the Hybrid Kit algorithm will be used as a baseline for comparison with the proposed algorithm. The Hybrid Kit algorithm belongs to the category of numerical algorithms described in Section 2.4.1.

Based on the motor speed error, the algorithm uses a PI-controller to generate a torque reference (T_e^{ref}). By using the Newton-Raphson iterative method on (2.13), which for convenience is repeated here

$$(L_q - L_d)^2 i_q^4 + \frac{2}{3p} T_e^{ref} \psi_m i_q - \left(T_e^{ref} \frac{2}{3p} \right)^2 = 0\,, \tag{4.3}$$

an approximated solution of the i_q current is found based on the requested torque T_e^{ref}. The corresponding i_d current is computed by using (2.12), which for convenience is repeated here

$$i_d = \frac{\psi_m}{2(L_q - L_d)} - \sqrt{\frac{\psi_m^2}{4(L_q - L_d)^2} + i_q^2}\,. \tag{4.4}$$

The parameters L_d, L_q, ψ_m are obtained as function of the i_d and i_q currents from the LuT data presented in Section 2.3. Notice that (4.3) and (4.4) are the result of neglecting the term T_d in (2.5), which can be source of inaccurate estimation of the MTPA trajectory. The proposed algorithm will be compared with the Hybrid Kit algorithm through the test scenarios described in the following section.

4.4 Test scenarios

The complete control system is evaluated on four different test scenarios presented below. For all scenarios the proposed algorithm will be compared with the Hybrid Kit algorithm described above. The comparison will be focused around the accuracy of the current angle β compared with the true MTPA found in Section 4.2.

4.4.1 Test 1: Steady state load torque variation

The first test intend to test the ability to track the parameter variations and MTPA operation at different current magnitude levels. The current magnitude is adjusted indirectly by changing the applied load torque. The system is tested for load torque ranging from about 20-90% of the maximum torque which corresponds to 40-140 Nm and each load torque level is kept for 1 s. For the entire test the reference speed is set to 300 rad/s while the load torque varies according to Figure 4.3.

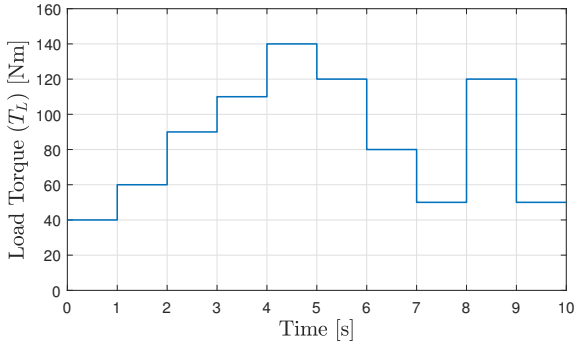

Figure 4.3: Applied load torque for test 1.

4.4.2 Test 2: Transient load torque variation

The second test aims to evaluate the ability to track the parameter variations and MTPA operation in transient conditions. Similarly to test 1, the load torque is varied between 40-140 Nm and the reference speed is set to 300 rad/s. The load torque variation is shown in Figure 4.4

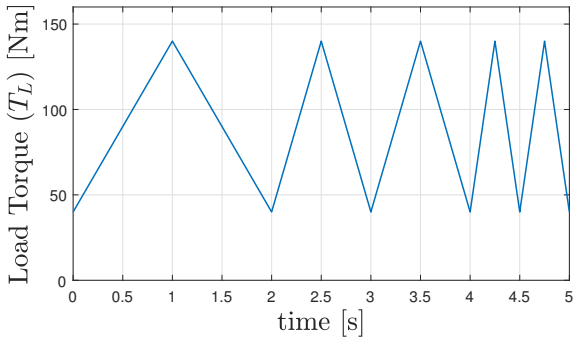

Figure 4.4: Applied load torque for test 2.

4.4.3 Test 3: WLTP driving scenario

The third test scenario is based on the Worldwide harmonized Light vehicles Test Procedure (WLTP) which is a standard driving cycle used in the industry. As MTPA only is applicable at below the rated motor speed only a small part of the low speed phase of the test is used. The vehicle speed profile provided by WLTP is converted to motor speed assuming the gear ratio is 1:5 and tire radius 0.2 m. The resulting reference motor speed profile is shown in Figure 4.5. The load torque is chosen as a function of the motor speed according to

$$T_L(\omega) = \frac{1}{3}\frac{2}{N_p}\omega\,, \tag{4.5}$$

where the factor $2/N_p$ is used to convert to mechanical rotation speed.

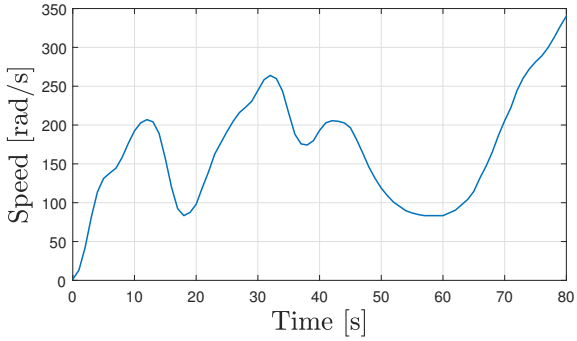

Figure 4.5: Reference speed profile for test 3. Data based on the low speed phase of the WLTP test.

4.4.4 Test 4: Incorrect LuT data in Signal Injection

The fourth test aims to further test the robustness to parameter variations and quantify the error obtained from using constant LuTs for the signal injection estimating $\hat{T}_d$, see Section 2.4.3. The test procedure is the same as in Test 1 however the VSI is supplied with erroneous parameter data. While the motor model uses the parameter data from the LuTs at 120° C, the virtual signal injection uses the LuT at 20° C. This should induce a small error in the parameter derivative estimations

and the final current angle β error should be of similar order of magnitude that can be expected from temperature variations.

5
Simulation results

In this chapter the simulation results for the thesis is shown. The performance of the proposed algorithm is compared with the default Hybrid Kit algorithm through the test scenarios described in Section 4.4. The results focuses on current angle tracking and parameter estimations.

5.1 Test 1: Steady state load torque variation

The reference speed tracking of the proposed control scheme for Test 1 is shown in Figure 5.1. It can be seen that the motor speed reaches the reference of 300 rad/s after each load torque step without overshoot. The error is less than 5 % of the reference speed for each of the load torque steps.

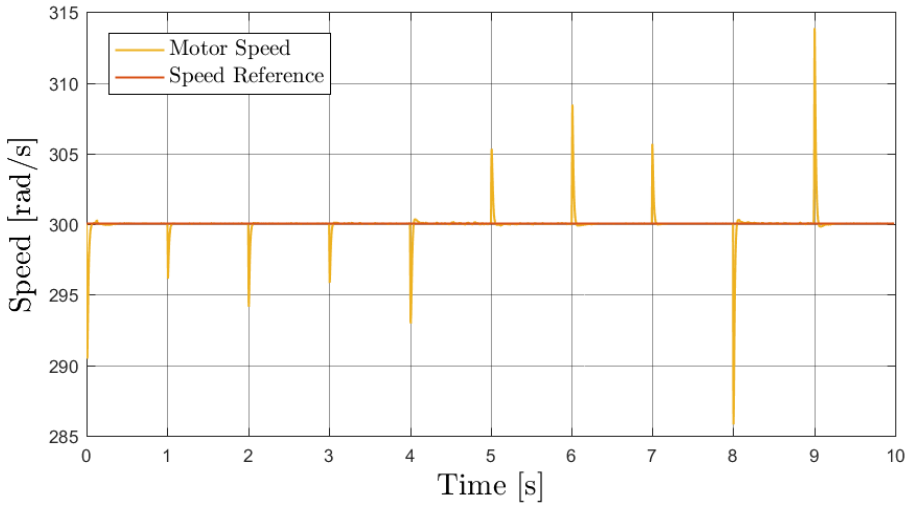

Figure 5.1: Reference speed tracking for the proposed algorithm during Test 1.

The parameter estimation results from Test 1 is shown in Figure 5.2. From the figure it can be seen that the control system estimates L_q with good performance for all torque levels. When it comes to ψ_m and L_d, the performance is overall good but the estimations are slightly noisier. However both parameters stay in a reasonable range of the real parameter value and the overall estimation is better then using the constant nominal values.

Both the ψ_m and L_d estimation starts off in the wrong direction as the load torque is decreased, see the steps at 5, 6, 7, and 9 seconds in Figure 5.2. This is likely to be

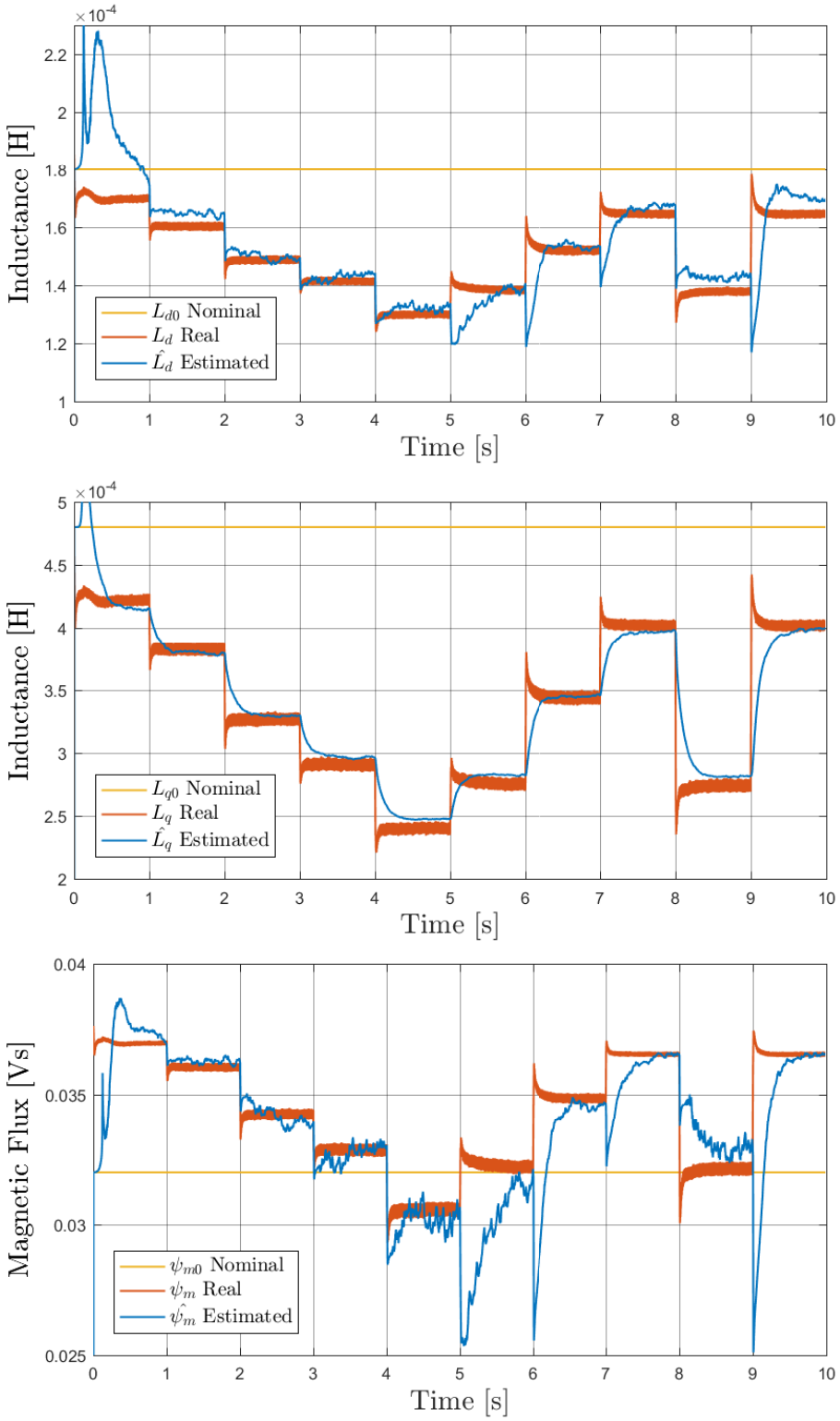

Figure 5.2: Parameter estimations for Test 1. The yellow line shown the constant parameter used in the reference model while the red and blue shows the true and estimated value respectively.

caused by the rapid change in load torque and should not be as severe of a problem in a real driving scenario.

The relatively large transient estimation errors in the beginning of Test 1 can be ignored as they are likely to be caused by the initial convergence of the P matrix in the RLS algorithm.

The resulting current angle β for Test 1 is shown in Figure 5.3. The β achieved by the proposed algorithm remains well within the 0.2 % error margin for almost the complete test. The algorithm also shows a quick rise time for β as the angle adopts to the new load torque level in about 0.1 second. The figure also shows that the proposed algorithm provides significantly better performance compared to the default Hybrid Kit algorithm. Note that the Hybrid Kit's β is only shown for steady state and hence no conclusion can be drawn about the transient behaviour for a load torque step.

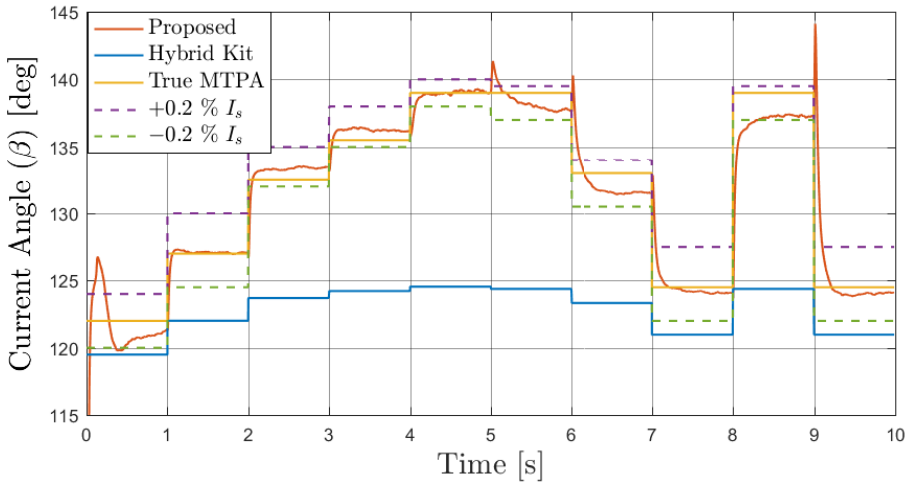

Figure 5.3: Resulting current angle β for step changes in the load torque (T_L) according to Test 1. The dashed support lines shown the β which results in ± 0.2 % current magnitude respectively. As a reference the resulting current angle from the Hybrid Kit is also shown.

5.2 Test 2: Transient load torque variation

The reference speed tracking of the proposed control scheme for Test 2 is shown in Figure 5.4. The figure shows that the motor speed is kept in a close region to the reference speed of 300 rad/s even when the load torque is changing rapidly at the end of the test.

The parameter estimation resulting from Test 2 is shown in Figure 5.6. From the figure it can once again be seen that the proposed algorithm manages to track the L_q parameter. The estimations have a small delay compared to the real value which is likely to be caused by the relatively high forgetting factor that is used in the RLS algorithm combined with the time needed to $\tilde{d}$ to convergence.

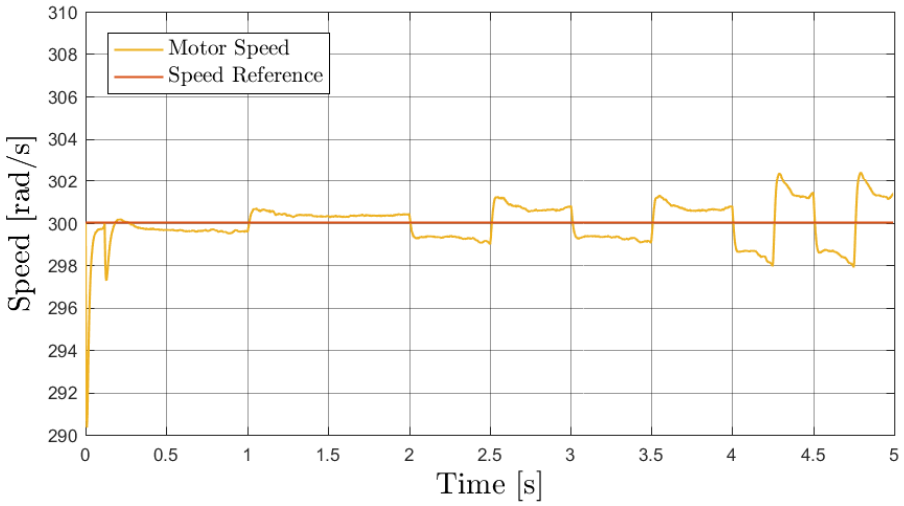

Figure 5.4: Reference speed tracking for the proposed algorithm during Test 1.

Similarly as in Test 1, the L_d and ψ_m estimations shows a bit worse transient behaviour after the discontinuous changes in load torque, especially when the load torque starts decreasing at 1, 2.5, 3.5, 4.25 and 4.75 seconds. However both parameters converges to a close region around the real value after some time of continuous change in load torque.

The resulting β angle for Test 2 is shown in Figure 5.5. The results show that the proposed algorithm manages to track β accurately even at the times when the parameters are estimated inaccurately. For a large portion of the test, the achieved β remains within the $\pm 0.2\%$ current magnitude error margin.

The default Hybrid Kit algorithm shows poor performance as the angle is far from the true MTPA, especially at the higher torque levels.

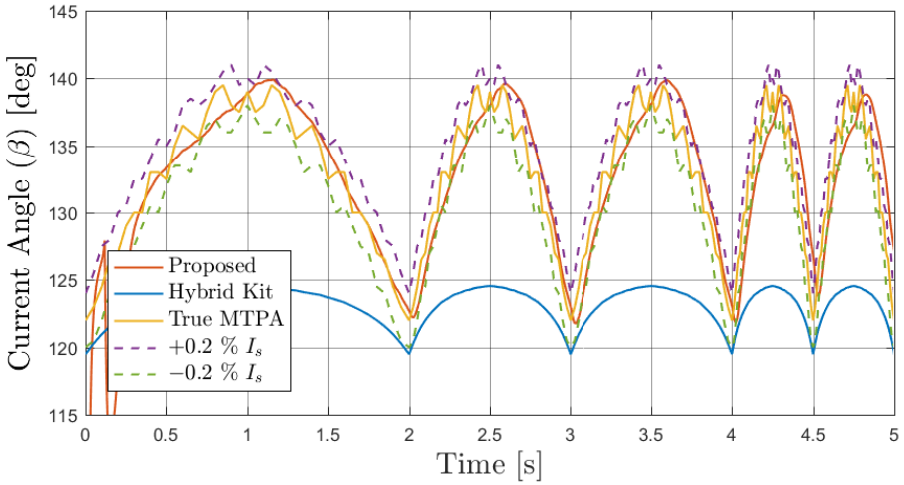

Figure 5.5: Resulting current angle β for step changes in the load torque (T_L) according to Test 2.

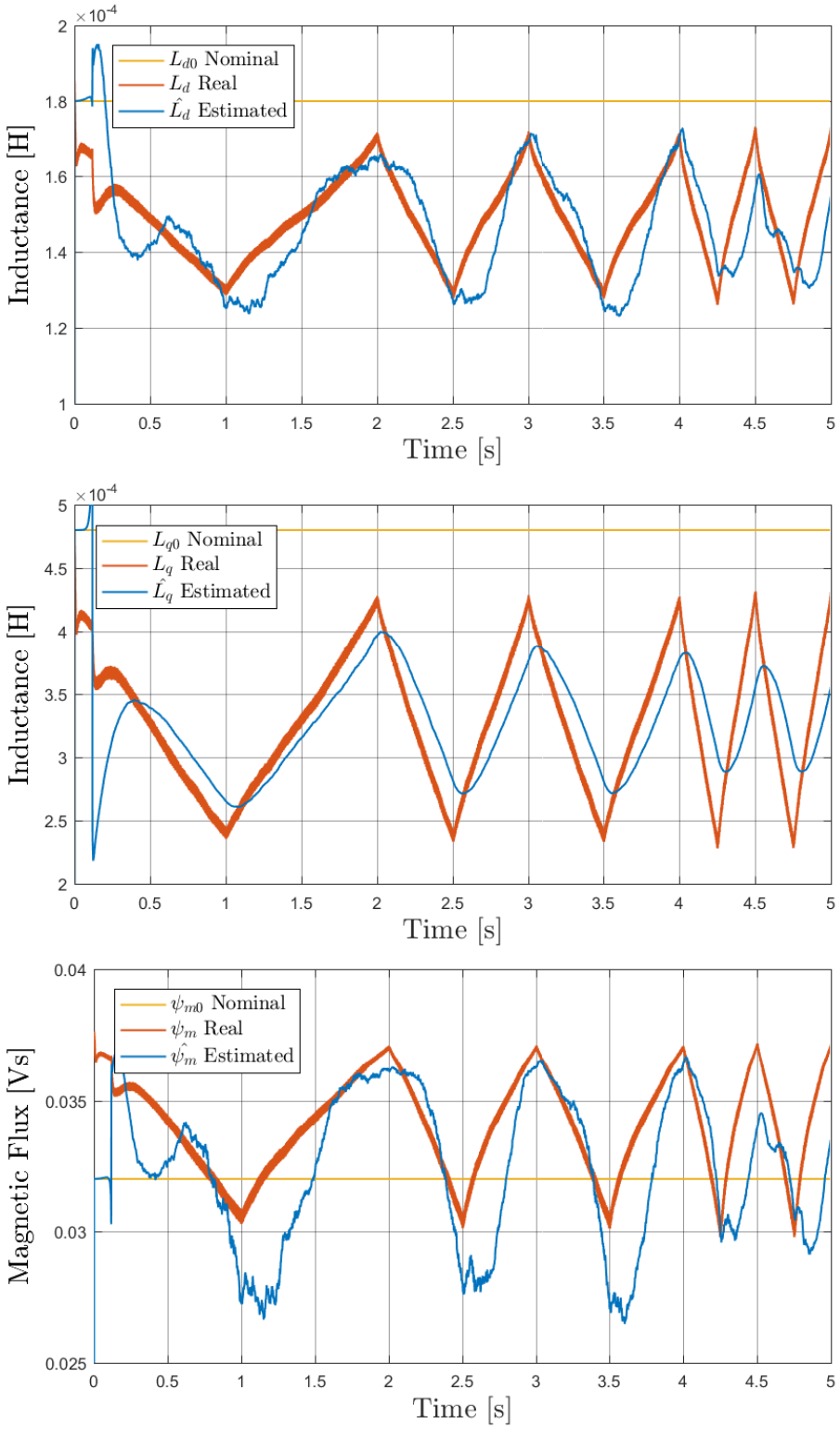

Figure 5.6: Parameter estimations for Test 2. The yellow line shown the constant parameter used in the reference model while the red and blue shows the true and estimated value respectively.

5.3 Test 3: WLTP driving scenario

The speed tracking error of the proposed algorithm for Test 3 is shown in Figure 5.7. From the figure it can be seen that the control scheme maintains good speed tracking throughout the speed range of the test.

The corresponding parameter estimations are shown in Figure 5.9. Both the L_d and ψ_m estimations show a small error at low speeds and hence low load torque levels. At these instances the estimation also oscillates more. The estimation L_q shows good tracking of the true value for the entire test session.

The resulting β angle for Test 3 is shown in Figure 5.8. The achieved β for the proposed algorithm follows the true MTPA for most of the processes. However at the instances when the motor speed is low ($\omega < 100$ rad/s), a small error occurs, which is probably caused by the error in the parameter estimations of L_d and ψ_m at this time.

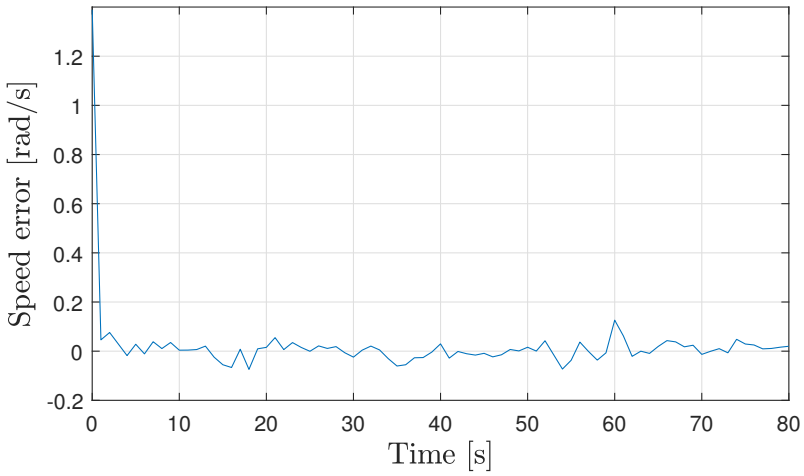

Figure 5.7: Speed tracking error for the proposed algorithm during Test 3.

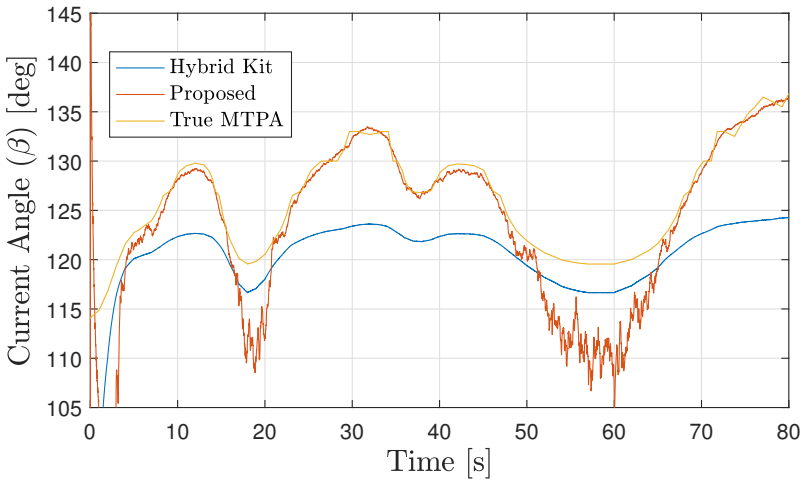

Figure 5.8: Resulting current angle β for step changes in the load torque (T_L) according to Test 3.

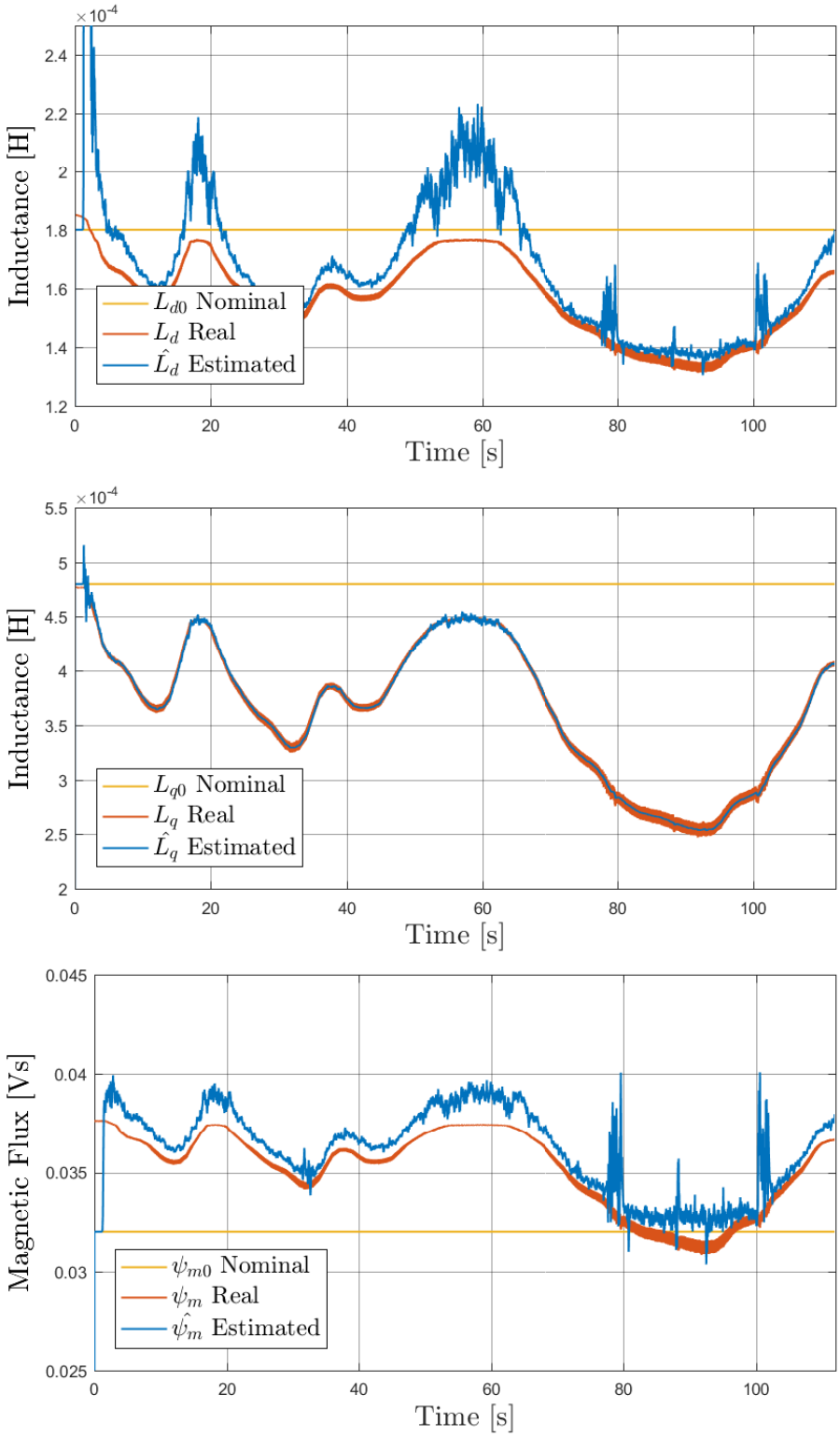

Figure 5.9: Parameter estimations for Test 3. The yellow line shown the constant parameter used in the reference model while the red and blue shows the true and estimated value respectively.

5.4 Test 4: Incorrect LuT data in Signal Injection

The difference in the parameter derivative estimations between using the correct (120 °C) and erroneous (20 °C) LuT for the VSI is shown in Figure 5.11. The figure shows small offsets in the inductance derivatives, especially for the d-axis. However the order of magnitude of the error is still rather small compared to the difference $\partial L_d/\partial\beta - \partial L_q/\partial\beta$ which is entered in the MTPA relation, see (2.7). For the magnet flux ψ_m, the difference between the two temperature levels is insignificant at all torque levels.

A comparison between the achieved current angle β for the two cases is shown in Figure 5.10. The figure shows that the effect on the MTPA tracking for using the wrong LuT is insignificant at all load torque levels.

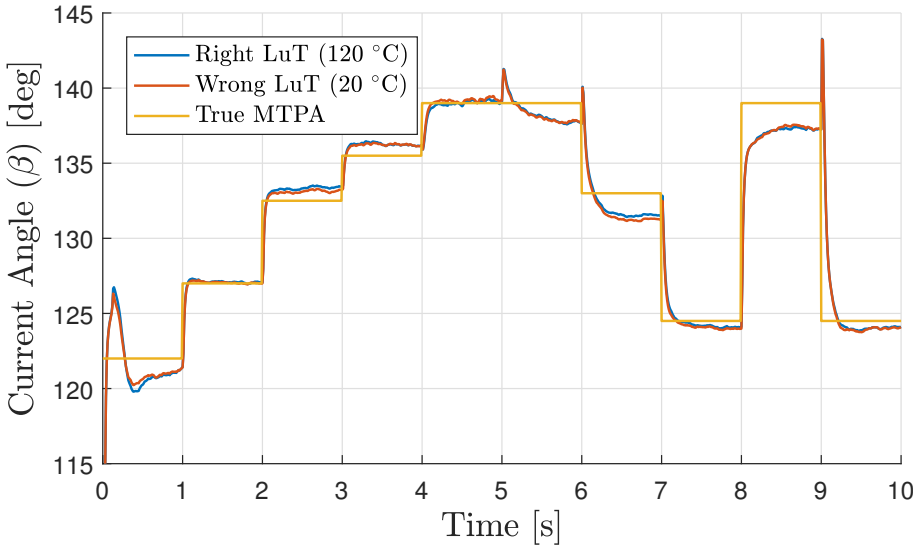

Figure 5.10: Current angle β tracking when using the same LuT as in the motor model compared to a LuT for another stator temperature.

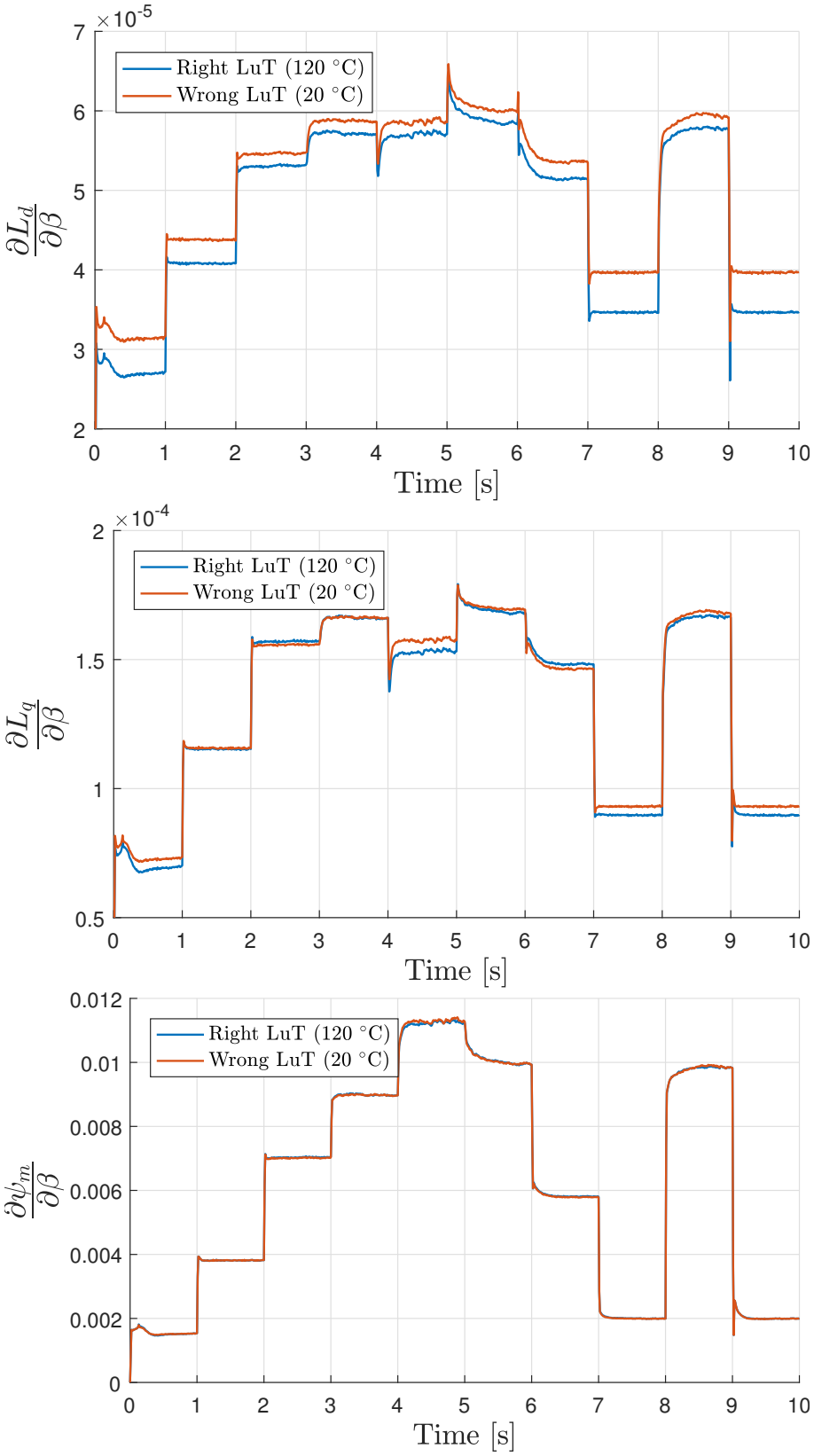

Figure 5.11: Parameter derivative estimations when using the same LuT as in the motor model compared to a LuT for another stator temperature.

6
Discussion

In this chapter the results presented above are discussed followed by a more general discussion around the MTPA problem. The proposed controller is analyzed and further development areas are discussed. The discussion lays the ground for the upcoming conclusion in next chapter.

6.1 Simulation Results

Overall the proposed control system demonstrate promising results both in terms of speed tracking, parameter estimations and MTPA accuracy. The MRAC technique provides good reference current tracking throughout the tested operation region as seen from the speed tracking result in both Test 1, 2 and 3.

In Test 1, the parameter estimation shows a quick step response of about 0.2 seconds which should be fast enough to track parameter variations in a vehicle application based on the analysis in Section 2.3. The convergence time seems to be heavily dependent on the convergence of $\tilde{\boldsymbol{d}}$ as the as error on the left hand side of (3.61) will result in erroneous estimations. This phenomena is likely to be the cause of the initial change in opposite direction to the true value in the parameter estimation which can be seen when the load torque decreases in Figure 5.2. An alternative approach would be to simply use the voltage equilibrium equations (2.1) for the parameter estimation and hence only use the $\tilde{\boldsymbol{d}}$ for the MRAC in order to maintain good reference current tracking throughout the operation range. This would also imply that compensation for the contributions of the nominal parts of the parameters in the current ripple estimation could be removed and (3.58) could be used directly in the RLS algorithm.

The L_d and ψ_m parameter estimations are in general more noisy compared to the L_q estimation. This is likely an effect of the properties of the $\boldsymbol{\varphi}$ matrix in (3.61). Slightly smoother estimations could be achieved using a larger forgetting factor in the RLS algorithm with a trade-off in convergence time. Moreover, the initial overshoot of the parameter estimation is likely due to the wrong initial value of the $\boldsymbol{P}$ matrix of the RLS algorithm given at the start of the simulation.

When it comes to Test 4, the proposed control scheme shows a promising robustness to temperature variations. The derivative of the parameters change insignificantly with respect to temperature and therefore using the erroneous LuTs has almost no effect on the resulting current angle. However the test does not provide any information in how well the control system handles aging of the machine as the phenomena may have a larger effect on the parameter derivatives.

6.2 Maximum Torque Per Ampere

In Section 4.2, the method and the result of the estimation of the true MTPA trajectory is presented. When comparing the result with other MTPA trajectories presented in other research papers [20, 21], it was noticed an unusual non-linear behaviour. After consulting with one of the Engineers at CEVT, it was concluded that it may be caused by the interpolation error of the LuTs that are used to model the motor. However, the trajectory presented in Figure 4.2 is still representative for the motor model used in the simulations and hence it can be used as a validation curve when comparing the control systems.

As described in 4.2, the Hybrid kit algorithm neglects the parameter derivative term T_d of (2.5) when solving the MTPA equation. From the result of the current angle estimation, presented in Figure 5.3 and 5.5, it is important to highlight the large error that neglecting this term generate on the current angle estimation. In fact, the difference between the Hybrid Kit's current angle estimation and the True MTPA can be traced back to the negligence of T_d as the parameters of the algorithm are the same as the once used in the motor model. It is therefore remarkable that most of the research papers in the area that was presented in Section 2.4 ignores the effect of this term. In some cases the authors have not even noticed the error as the MTPA accuracy merely was concluded based on the accuracy of the parameter estimations [27, 23].

6.3 Proposed Control System

When analyzing the balance between complexity and MTPA estimation accuracy, it is worth comparing the proposed algorithm with the VSI method. As mentioned in Section 2.4.3, the VSI technique generally do a great job in tracking MTPA compared to other methods. Since both the proposed control scheme and the VSI techniques uses LuTs for estimating the variation of the parameter with respect to the current angle, they are expected to have similar MTPA accuracy. For the time being, the proposed control scheme estimates the derivative terms using constant LuTs for the parameters. As the parameters change over time, these will not be representative anymore and, for having a completely parameter independent control scheme that tracks MTPA, another approach would be needed. As opposed to signal injection methods, the proposed algorithm could use the information from the parameter estimations to update the LuTs over time. This would give the opportunity to have the same performance even if the initial LuTs are not representative of the motor characteristic. However, the implementation of such a system could lead to added complexity. Since the parameter estimation usually run close to the MTPA operation and as the derivative terms show an important effect on the correct tracking of the MTPA, a compensation should be considered in order to keep the derivative terms accurate. Therefore, the increase in accuracy in the long term can be done at the expense of complexity, which would make the integration of the proposed method in a vehicle powertrain more challenging.

Another aspect that may limit the integration of the proposed control system is

the measurement of the current ripple. As the algorithm requires multiple precise measurement of the current during each switching period (8 kHz) of the inverter, as presented in Section 3.3.2, the hardware needs to be selected accordingly. The adopted current noise level of about 0.2 % of the max current also puts requirements on the hardware. During the tuning of the controller it was observed that larger noise magnitudes caused problems for the L_d and ψ_m estimations which already are rather sensitive as seen in the estimation results. Even if sensor noise was added in the motor model, there is still an uncertainty factor of how well the simulation represents a real test case.

Because of the complexity of the complete system and all dependencies between the different subsystems, it is hard to guarantee the stability of the complete system. If an error is introduced in the parameter estimation, the solution in the MTPA equation may result in a very small current angle. The small current angle results in a low d-axis current magnitude which in turn affects the condition number for the $\boldsymbol{\varphi}$ matrix in the parameter estimation and result in a even larger parameter estimation error. In this way, a small error can quickly propagate through the system and amplify itself. Stopping the RLS algorithm when the motor speed or current levels are too low is a first step to avoid these and similar problems in the simulation environment. However for testing on a real system safety features like this must be much more rigorously developed and verified through a broad set of test scenarios.

Because of the observed parameter estimation accuracy in steady state, the proposed parameter estimation scheme is also demonstrating a great potential as a stand alone algorithm. The estimation technique could potentially be used as an alternative to directly measuring the motor parameters in a benching process. As the algorithm only requires the standard current, voltage and motor speed measurements, no additional equipment would be needed in the bench setup. Using the estimated parameters, the produced torque could be calculated and compared with the measured torque as a validation step.

7
Conclusion

This thesis focused on developing an algorithm for an accurate estimation and tracking of the MTPA of an IPMSM. Based on the literature study, various methods have been investigated and a novel algorithm has been developed. The proposed method is based on MRAC that, combined with a current ripple modelling, allows full real time motor parameter estimations. For additional MTPA accuracy, a VSI technique is implemented in combination with parameter LuTs to estimate the parameter derivatives with respect to the current angle. The proposed method is designed to be independent of the IPMSM parameters and is able to accurately track parameter variations and maintain good MTPA accuracy over time. However, the signal injection method uses LuT data of the parameters in order to estimate how they vary with the derivative of the current angle, so the method is not fully adaptive.

The evaluation of the performance has been done in a simulation environment by comparing the proposed method with a default Hybrid Kit algorithm that currently is used by the company. Based on the reference of the true MTPA of the motor model, the proposed method shows significantly better performance in MTPA estimation with close to perfect tracking of the true MTPA throughout the operation region.

7.1 Future Work

Based on the findings of this thesis, looking into the following topics could be a start for further development of the control scheme.

Investigate how the parameter estimation performance could be improved by directly using the voltage equilibrium in (2.1) instead of the estimated model error between the reference and real model $\tilde{\boldsymbol{d}}$.

In order to make the algorithm work entirely without prior knowledge of the IPMSM, the LuTs method used in the signal injection needs to be revised. This could be achieved by integrating adaptive LuTs that are updated with the help of the parameter estimation scheme.

Further look into the stability of the complete control scheme and the interventions that are needed to ensure that, e.g. preventing an error from the parameter estimation to propagate and amplify itself.

Finally, as the results of this thesis only are based on simulation experiments, a natural follow up would be to test the control system with hardware in the loop.

Bibliography

[1] L. Harnefors, *Control of Variable-speed Drives*. Applied Signal Processing and Control, Department of Electronics, Mälardalen University, 2002.

[2] B. Chalmers, *Electric Motor Handbook*. Butterworth-Heinemann, 1988.

[3] M. Barcaro, *Design and Analysis of Interior Permanent Magnet Synchronous Machines for Electric Vehicles*. PhD thesis, University of Padova, 2011.

[4] S. A. N. Ion Boldea, *Electric Drives second edition*. 6000 Broken Sound Parkway NW, suite 300: Taylor & Francis Group, 2006.

[5] T. M. Jahns, G. B. Kliman, and T. W. Neumann, "Interior permanent-magnet synchronous motors for adjustable-speed drives," *IEEE Transactions on Industry Applications*, vol. IA-22, pp. 738–747, July 1986.

[6] S. Li, B. Sarlioglu, S. Jurkovic, N. R. Patel, and P. Savagian, "Comparative analysis of torque compensation control algorithms of interior permanent magnet machines for automotive applications considering the effects of temperature variation," *IEEE Transactions on Transportation Electrification*, vol. 3, pp. 668–681, Sep. 2017.

[7] Q. Liu, A. Thul, and K. Hameyer, "A robust model reference adaptive controller for the pmsm drive system with torque estimation and compensation," in *2014 International Conference on Electrical Machines (ICEM)*, pp. 665–671, Sep. 2014.

[8] K. Choi, Y. Kim, K. Kim, and S. Kim, "Using the stator current ripple model for real-time estimation of full parameters of a permanent magnet synchronous motor," *IEEE Access*, vol. 7, pp. 33369–33379, 2019.

[9] T. Sun, M. Koç, and J. Wang, "Mtpa control of ipmsm drives based on virtual signal injection considering machine parameter variations," *IEEE Transactions on Industrial Electronics*, vol. 65, pp. 6089–6098, Aug 2018.

[10] D. B.-B. C. B. Fleur Scheele, Emmanuel Umpula Nkumba, "Cobalt blues," *SOMO Centre for Research on Multinational Corporations*, 2016.

[11] S. Amornwongpeeti, O. Kiselychnyk, J. Wang, C. Antaloae, M. Soumelidis, and N. Shah, "A combined mtpa and maximum efficiency control strategy for ipmsm motor drive systems," in *2016 International Conference on Electrical Systems for Aircraft, Railway, Ship Propulsion and Road Vehicles International Transportation Electrification Conference (ESARS-ITEC)*, pp. 1–6, Nov 2016.

[12] S. Amornwongpeeti, O. Kiselychnyk, J. Wang, C. Antaloae, M. Soumelidis, and N. Shah, "A combined mtpa and maximum efficiency control strategy for ipmsm motor drive systems," in *2016 International Conference on Electrical Systems for Aircraft, Railway, Ship Propulsion and Road Vehicles International Transportation Electrification Conference (ESARS-ITEC)*, pp. 1–6, Nov 2016.

[13] S. Morimoto, Y. Tong, Y. Takeda, and T. Hirasa, "Loss minimization control of permanent magnet synchronous motor drives," *IEEE Transactions on Industrial Electronics*, vol. 41, pp. 511–517, Oct 1994.

[14] K. D. Hoang, Z. Q. Zhu, and M. Foster, "Online optimized stator flux reference approximation for maximum torque per ampere operation of interior permanent magnet machine drive under direct torque control," in *6th IET International Conference on Power Electronics, Machines and Drives (PEMD 2012)*, pp. 1–6, March 2012.

[15] K. D. Hoang, J. Wang, M. Cyriacks, A. Melkonyan, and K. Kriegel, "Feedforward torque control of interior permanent magnet brushless ac drive for traction applications," in *2013 International Electric Machines Drives Conference*, pp. 152–159, May 2013.

[16] Y. Kim and S. Sul, "Torque control strategy of an ipmsm considering the flux variation of the permanent magnet," in *2007 IEEE Industry Applications Annual Meeting*, pp. 1301–1307, Sep. 2007.

[17] H. Kim, Y. Lee, S. Sul, J. Yu, and J. Oh, "Online mtpa control of ipmsm for automotive applications based on robust numerical optimization technique," in *2018 IEEE Transportation Electrification Conference and Expo (ITEC)*, pp. 442–447, June 2018.

[18] Y. Miao, H. Ge, M. Preindl, J. Ye, B. Cheng, and A. Emadi, "Mtpa fitting and torque estimation technique based on a new flux-linkage model for interior-permanent-magnet synchronous machines," *IEEE Transactions on Industry Applications*, vol. 53, pp. 5451–5460, Nov 2017.

[19] M. Preindl and S. Bolognani, "Optimal state reference computation with constrained mtpa criterion for pm motor drives," *IEEE Transactions on Power Electronics*, vol. 30, pp. 4524–4535, Aug 2015.

[20] S. Kim, Y. Yoon, S. Sul, K. Ide, and K. Tomita, "Parameter independent maximum torque per ampere (mtpa) control of ipm machine based on signal injection," in *2010 Twenty-Fifth Annual IEEE Applied Power Electronics Conference and Exposition (APEC)*, pp. 103–108, Feb 2010.

[21] T. Sun, J. Wang, and X. Chen, "Maximum torque per ampere (mtpa) control for interior permanent magnet synchronous machine drives based on virtual signal injection," *IEEE Transactions on Power Electronics*, vol. 30, pp. 5036–5045, Sep. 2015.

[22] J. Wang, X. Huang, D. Yu, Y. Chen, J. Zhang, F. Niu, Y. Fang, W. Cao, and H. Zhang, "An accurate virtual signal injection control of mtpa for an ipmsm with fast dynamic response," *IEEE Transactions on Power Electronics*, vol. 33, pp. 7916–7926, Sep. 2018.

[23] X. Z. Z. M. X. L. Yang Yu, Da Chang and C. Sun, "Adaptive backstepping based mtpa sensorless control of pm-assisted synrm with fully uncertain parameters," *Mathematical Problems in Engineering*, vol. 2018, 2018.

[24] Y. Yu, Z. Mi, X. Zheng, D. Chang, X. Zheng, and C. Sun, "Adaptive sliding mode backstepping control - based maximum torque per ampere control of permanent magnet-assisted synchronous reluctance motor via nonlinear disturbance observer," *Advances in Mechanical Engineering*, vol. 10, no. 7, 2018.

[25] G. M. Schoonhoven and M. N. Uddin, "Mtpa and fw based robust nonlinear speed control of ipmsm drive using lyapunov stability criterion," in *2014 IEEE Industry Application Society Annual Meeting*, pp. 1–8, Oct 2014.

[26] Q. Liu and K. Hameyer, "High-performance adaptive torque control for an ipmsm with real-time mtpa operation," *IEEE Transactions on Energy Conversion*, vol. 32, pp. 571–581, June 2017.

[27] Q. Liu and K. Hameyer, "An adaptive torque controller with mtpa for an ipmsm using model based self-correction," in *IECON 2014 - 40th Annual Conference of the IEEE Industrial Electronics Society*, pp. 391–397, Oct 2014.

[28] A. I. J. v. E. S. M. T. M. Krstic, *Adaptive Control Algorithms, Analysis and Applications*. Springer, 2011.

[29] L. Harnefors and H. . Nee, "Model-based current control of ac machines using the internal model control method," *IEEE Transactions on Industry Applications*, vol. 34, pp. 133–141, Jan 1998.

[30] H. K. Khalil, *Nonlinear systems; 3rd ed.* Upper Saddle River, NJ: Prentice-Hall, 2002.

[31] R. Jeyabalan, *Evaluation of microcontroller architectures for PMSM control*. Master's thesis, Chalmers University of Technology, Göteborg, Sweden, 2015.

[32] T. Sun, J. Wang, and X. Chen, "Maximum torque per ampere (mtpa) control for interior permanent magnet synchronous machine drives based on virtual signal injection," *IEEE Transactions on Power Electronics*, vol. 30, pp. 5036–5045, Sep. 2015.

A

Park-Clarke Transformation

Park-Clarke transformations are used to transform quantities between the fixed three phase abc-reference frame and the rotating direct-quadrature dq-reference frame [4]. The relation between the reference frames are illustrated in Figure A.1.

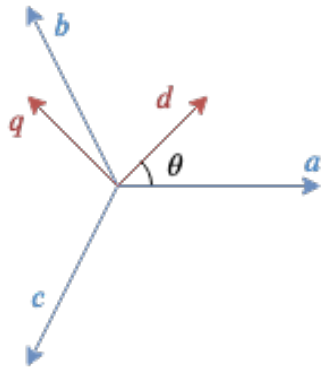

Figure A.1: Relation between the dq and abc reference frame.

A.1 Park Transformation

In order to describe the dynamics of the motor the three-phase quantities are transformed into the dq-frame through the Park transformation

$$\begin{bmatrix} d \\ q \end{bmatrix} = \sqrt{\frac{2}{3}} \begin{bmatrix} \cos(\theta) & \cos(\theta - \frac{2\pi}{3}) & \cos(\theta + \frac{2\pi}{3}) \\ \sin(\theta) & \sin(\theta - \frac{2\pi}{3}) & \sin(\theta + \frac{2\pi}{3}) \end{bmatrix} \begin{bmatrix} a \\ b \\ c \end{bmatrix} \tag{A.1}$$

where θ is the instantaneous angle from the a-axis to the rotating d-axis.

A.2 Clarke Transformation

The inverse transformation from the direct-quadrature to the three phase components is know as Clarke transformation and is described by the matrix operation

$$\begin{bmatrix} a \\ b \\ c \end{bmatrix} = \sqrt{\frac{2}{3}} \begin{bmatrix} \cos(\theta) & -\sin(\theta) \\ \cos\left(\theta - \frac{2\pi}{3}\right) & -\sin\left(\theta - \frac{2\pi}{3}\right) \\ \cos\left(\theta + \frac{2\pi}{3}\right) & -\sin\left(\theta + \frac{2\pi}{3}\right) \end{bmatrix} \begin{bmatrix} d \\ q \end{bmatrix} \tag{A.2}$$

B

Recursive Least Square Algorithm

Given a linear system of the form

$$\boldsymbol{y} = \boldsymbol{\varphi}\boldsymbol{\theta} \tag{B.1}$$

the RLS algorithm can be summarized in the following equations

$$\boldsymbol{K}(n) = \boldsymbol{P}(n-1)\boldsymbol{\varphi}^T \left(\lambda \boldsymbol{I} + \boldsymbol{\varphi}(n)\boldsymbol{P}(n-1)\boldsymbol{\varphi}(n)\right)^{-1} \tag{B.2}$$

$$\hat{\boldsymbol{\theta}}(n) = \hat{\boldsymbol{\theta}}(n-1) + \boldsymbol{K}(n)\left(\boldsymbol{y}(n) - \boldsymbol{\varphi}(n)\hat{\boldsymbol{\theta}}(n-1)\right) \tag{B.3}$$

$$\boldsymbol{P}(n) = \frac{1}{\lambda}\left(\boldsymbol{I} - \boldsymbol{K}(n)\boldsymbol{\varphi}(n)\right)\boldsymbol{P}(n-1) \tag{B.4}$$

where λ is a positive forgetting factor < 1.